Scanning Microscopy Vol. 12, No. 3, 1998 (Pages 415-436) 0891-7035/98$5.00+.25
Scanning Microscopy International, Chicago (AMF O'Hare), IL 60666 USA

ELECTRON DIFFRACTION BY CARBON NANOTUBES

A.A. Lucas[1]*, V. Bruyninckx[1], Ph. Lambin[1], D. Bernaerts[2], S. Amelinckx[2], J. Van Landuyt[2] and G. Van Tendeloo[2]

[1]Department of Physics, Facultés Universitaires Notre-Dame de la Paix, Namur, Belgium
[2]EMAT, University of Antwerp (RUCA), Belgium

(Received for publication July 18, 1996 and in revised form January 28, 1997)

Abstract

This paper first presents results from electron diffraction (ED) and transmission electron microscopy (TEM) of carbon nanotubes. TEM and ED of straight or coiled nanotubes are shown and the mechanisms of formation of the diffraction patterns caused by their specific atomic structures are qualitatively explained. Then a quantitative theory of kinematical diffraction by straight carbon nanotubes is proposed. The formalism is inspired from the theory of X-Ray diffraction by helical structures originally developed by Cochran, Crick and Vand for biological molecules. Each of the cylindrical graphene layers in a nanotube is viewed as being constructed from a finite set of regularly spaced carbon helices sharing the nanotube axis. This description leads to an exact, compact formula for the total kinematical diffraction amplitude of a complete monolayer tubule of arbitrary chirality. We illustrate the theory with computer simulations of the diffraction patterns of monolayer tubules and multilayer nanotubes of mixed chiralities and compare with observed ED patterns. The closed-form formula for the scattering amplitude of a single tubule also provides the molecular form factor to further compute the diffraction by the regular lattice of parallel tubules observed recently. We finally indicate briefly how the method can be extended to compute the kinematical diffraction by coiled nanotubes and other helical structures of nanometer size.

Key Words: Carbon nanotubes, transmission electron microscopy, electron diffraction, helical structures.

*Address for correspondence:
A.A. Lucas
Facultés Universitaires Notre-Dame de la Paix
rue de Bruxelles 61
B-5000 Namur, Belgium
Telephone number: + 32 81 72 47 08
Fax number: + 32 81 72 47 07
E-mail: amand.lucas@scf.fundp.ac.be

Introduction

It has been realized in the past ten years that pure elemental carbon can condense in a variety of new three-dimensional structures different from the traditional crystalline sp^2 planar graphite and sp^3 diamond. When a high-temperature carbon vapor cools down and condenses in an inert atmosphere (Kroto *et al.*, 1985; Krätschmer *et al.*, 1990) spheroidal, closed-cage carbon clusters called fullerenes are formed with predominantly sp^2 bonding between the atoms, the most celebrated example being the truncated-icosahedron shaped C_{60} molecule first identified by Kroto *et al.*, (1985). In addition to these globular fullerenes, other types of sp^2 bonded clusters were discovered, in particular hollow carbon fibers of micrometer lengths and nanometer diameters. Iijima (1991) was the first to observe these tubular fullerenes in the electrode deposit formed in the carbon-arc method of fullerene production (Krätschmer *et al.*, 1990). Using transmission Electron Diffraction (ED) and high-resolution Transmission Electron Microscopy (TEM), he could demonstrate that the nanotubes consist of a few individual graphene sheets rolled up into coaxial circular cylinders of nanometer diameters and that the seamless cylinders are separated by the canonical graphitic interlayer distance of about 3.4 Å. Ebbesen and Ajayan (1992) succeeded in adjusting the conditions of the carbon-arc evaporation to make nanotubes in large quantities. The nanotubes can be purified from undesirable soot components by controlled oxidation (Ebbesen *et al.*, 1994). Shortly after the discovery of the multilayer nanotubes, Iijima and Ichihashi (1993) and Bethune *et al.*, (1993) were able to produce, in a carbon-arc generator, abundant amounts of single-wall, or monolayer tubules by co-evaporating a transition metal (e.g., Fe or Co) along with carbon. Iijima and Ichihashi (1993) managed to obtain ED and TEM pictures of such a single-wall tubule. The reader is referred to Ebbesen (1994) for a review of nanotube (carbon-arc) synthesis and properties.

Among the most detailed TEM and ED studies of the morphology of straight multilayer nanotubes are those reported by Zhang *et al.* (1993a,b) and by Liu and Cowley (1994a,b). A few selected examples will be discussed.

A different approach to carbon nanotube synthesis is the low-temperature, catalytic growth method which was used

by José-Yacaman *et al.* (1993) and by Ivanov *et al.* (1994). This method, which consists in the cracking of hydrocarbons on the surface of a finely divided metal catalyst, was already in widespread use for the catalytic production of mesoscopic carbon fibers (reviews of which are given by: Dresselhaus *et al.*, 1988; Baker, 1989; Rodriguez, 1993). Ivanov *et al.* (1994) showed that in the appropriate synthesis conditions, besides the straight nanotubes, several weight percent of regularly coiled nanotubes were co-synthesized by the catalyst. Apart from their size, the coiled nanotubes appear to be similar to the coiled carbon filaments of mesoscopic diameters previously observed (see Kawaguchi *et al*., 1992, and references therein). TEM and ED studies (Ivanov *et al.*, 1994; Zhang *et al.*, 1994) have shown that, like globular fullerenes, the coiled as well as the straight, catalytically grown nanotubes when properly annealed and purified are hollow and have a degree of graphitization comparable to that of the carbon-arc grown species which makes them suitable for observation by high-resolution electron microscopy and diffraction.

A further method of nanotube synthesis is by electrolysis (Hsu *et al.*, 1995).

A number of papers have been devoted to the possible growth mechanisms for straight or coiled nanotubes (Amelinckx *et al.*, 1994, 1995b; Colbert *et al.*, 1994; Gamaly and Ebbesen, 1995; Fonseca *et al.*, 1995; Guo *et al.*, 1995a,b; Colbert and Smalley, 1995) but these will not be discussed here.

Nanotubes are of great interest for their novel structural (Dresselhaus *et al.*, 1992), electronic (Hamada *et al.*, 1992; Mintmire *et al.*,, 1992; Charlier and Michenaud, 1993; Lambin *et al.*, 1995; Langer *et al.*, 1995), optical (Hiura *et al.*, 1993; Bacsa and De Heer, 1995; Henrard *et al.*, 1996), magnetic (Lu, 1995) and other properties. For practical applications, they are expected to exhibit mechanical properties (Robertson *et al.*, 1992) approaching the theoretical limit for sp^2 bonded carbon and could lead to composite materials superior in strength to those prepared with the macroscopic and mesoscopic carbon fibers in current industrial usage (Dresselhaus *et al.*, 1988).

In the rest of this paper, we concentrate on the two techniques best suited for ascertaining the structural characteristics of a single nanotube, namely TEM and ED. We examine a few typical TEM and ED micrographs of straight or coiled nanotubes. We discuss qualitatively the mechanisms by which the micrographs are generated from the scattering of electrons by the assumed atomic structure of the nanotubes. Then we present a mathematical theory for the calculation of electron scattering in the first Born, or kinematical approximation. Computer simulations based on the theory will be shown to successfully predict the principal features of the diffraction patterns observed experimentally for straight nanotubes. Finally we indicates in outline how the theory can be extended to obtain the diffraction from coiled nanotubes (Ivanov *et al.*, 1994) as well as from other helical structures of light atoms such as the conical scroll carbon fibers recently revealed by ED (Amelinckx *et al.*, 1992).

TEM and ED micrographs of nanotubes

In this section, we present selected TEM and ED micrographs of straight or coiled nanotubes and explain in simple terms the major characteristic features arising from the underlying atomic structures.

In order to avoid confusion, throughout the rest of this paper, we will systematically use the word *tubule* to refer to a carbon tube having one single graphene layer while the word *nanotube* will be reserved for multiwall tubes.

Straight nanotubes

Figure 1 reproduces the original micrographs obtained by Iijima (1991) for a straight nanotube. Figure 1a shows two parallel sets of 7 lines separated by a uniform region. The lines are lattice fringes generated by the electron beam running approximately perpendicular to the axis of the 7-layers, hollow, circular nanotube. The electrons channel between the quasi-planar sheets of the carbon honeycomb lattice parallel to the beam on either sides of the nanotube. The outer and inner diameters of the nanotube are 6.5 nm and 2.2 nm, respectively, and the layers are separated by the graphitic distance of 0.34 nm. In effect, Figure 1a represents a projection of the structure in the beam direction. The corresponding diffraction pattern is presented in Figure 1b. There are two sets of spots organized in mm2 mirror symmetry about the projection of the nanotube axis. The bright, equidistant spots labeled (0002m) are aligned perpendicular to the nanotube axis. They are produced by the diffraction from the two sets of parallel quasi-planes whose projections are shown in Figure 1a and which act as line gratings for the electron waves. The other set of spots arranged in circles around the transmitted(0000) beam is produced by the diffraction of the two stacks of 7 hemi-cylindrical layers upstream and downstream of the beam. The first-order circle in Figure 1b comprises three hexagonal sets of spots.

To understand the details of the pattern, one must take account of the possible chiral arrangement of atoms in the successive tubules of the nanotube (Iijima, 1991). When constructing a seamless cylinder by rolling up a piece of graphene as shown in Figure 2a, one can obtain an achiral or a chiral tubule depending on whether the free edges are sealed without (Fig. 2b,c) or with (Fig. 2d) an integer offset of the honeycomb network along the seam. An achiral tubule can be either of the "perpendicular" type (i.e. having one set of C-C bonds perpendicular to the tube axis, Fig. 2b) or of the "parallel" type (C-C bonds parallel to the axis, Fig. 2c). Chiral tubules are characterized by a chiral angle α which is proportional to the quantized hexagon offset introduced at the seam (Fig. 2d). There are several ways to define α but in the present paper we shall use the angle between the tubule diameter and the nearest

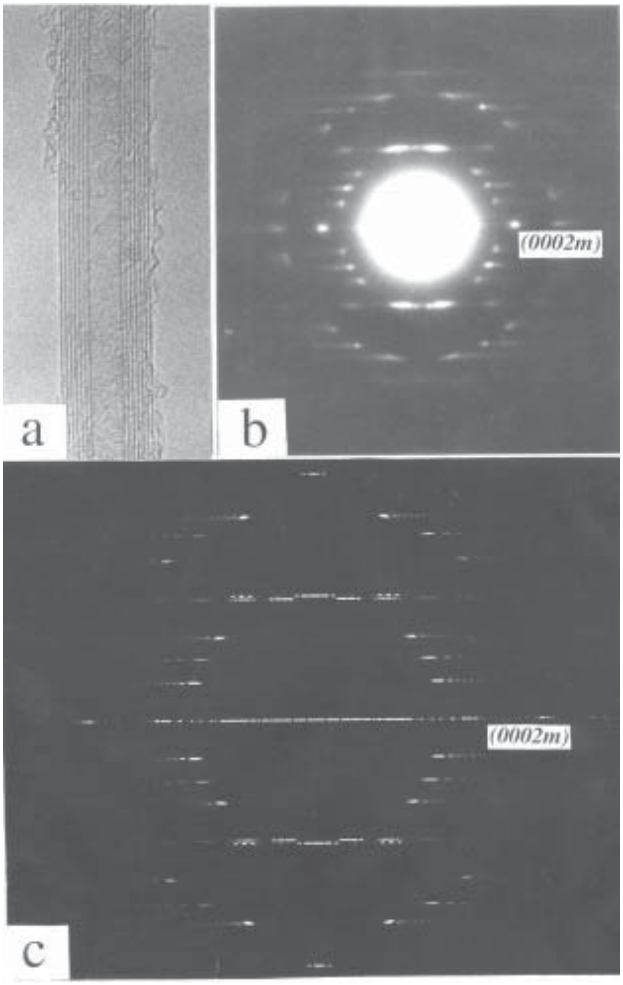

Figure 1. (**a**) Bright-field TEM image of a 7-layers nanotube; the 0.34 nm distance between the fringes sets the distance scale. (**b**) Observed diffraction pattern for the nanotube in a (Iijima, 1991). (**c**) Computer simulated pattern for a model 7-layers nanotube made of the successive (29,0), (38,0), (47,0), (48,13), (55,16), (63,17), (70,20) tubules, having radii increasing by about 0.34 nm (the (L,M) tubule notation is made clear in Figure 2a). The small vertical splitting of the chiral streaks is caused by the slightly different chiral angle of about 12° of the outer four tubules. The spots marked (0002m) and the intervening intensity modulation are produced by the vertical double diffraction grating of Figure 1a.

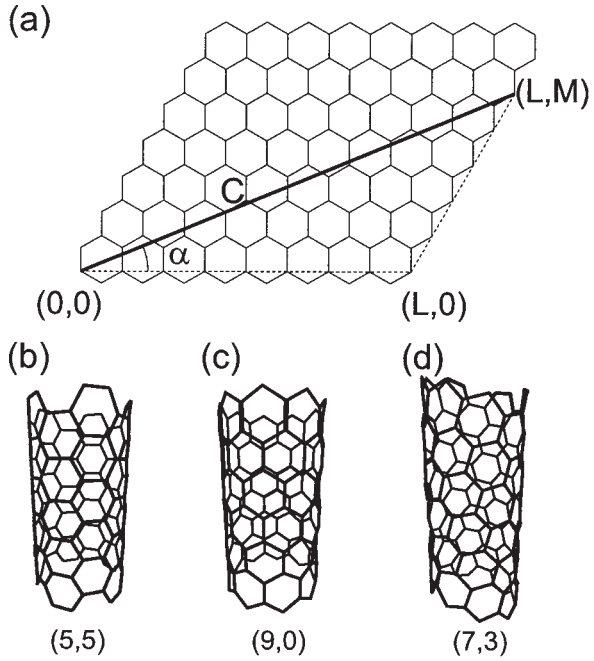

Figure 2. (**a**) Definition of an (L,M) tubule in a graphene sheet (Hamada *et al.*, 1992); the tubule is obtained by rolling up the sheet and superposing the (L,M) site with the (0,0) site. C is the tubule circumference and a is its chiral angle. (**b**) Achiral (5,5) "perpendicular" tubule. (**c**) Achiral (9,0) "parallel" tubule. (**d**) Chiral (7,3) tubule.

zig-zag line of atoms, as shown in Figure 2a.

Achiral tubules produce a hexagonal set of diffraction spots (middle hexagon in Fig. 1b) having the (projection of the) tube axis as symmetry axis. The observed spots are not the usual circular diffraction features characteristic of 3-D crystalline materials but are diffuse, comma-shape streaks elongated normal to the tube axis and fading away from the axis (the origin of the streaking will be explained below). In Figure 1b, the middle hexagon of the set of three in the first-order circle has two edges lying parallel to the tube axis. These spots originate from one or several achiral, parallel tubules (Fig. 2c). The absence in Fig. 1b of a hexagon of first order spots with edges perpendicular to the tube axis indicates the absence of perpendicular tubules (Fig. 2b) in this nanotube.

A chiral tubule on the other hand will produce two hexagonal sets of streaked spots rotated symmetrically with respect to the previous achiral set. One hexagon is the result of diffraction by the upstream, hemi-cylindrical portion of the tube and the other by the downstream part. The rotation angle separating the two hexagons is twice the chiral angle α in Figure 2a. In Figure 1b, one clearly observes a pair of hexagons of streaked spots in the first order circle symmetrically placed with respect to the achiral spots and rotated with respect to the latter by a chiral angle α of about 12°.

Figure 3 shows a diffraction pattern obtained by Zhang *et al.* (1993b) from the nanotube shown in Figure 3a. The electron beam is perpendicular to the nanotube axis. The

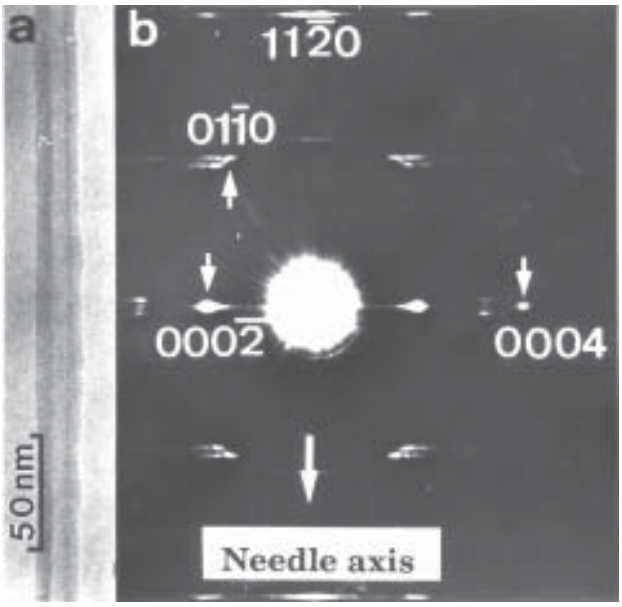

Figure 3. (**a**) Bright-field image of a thick multilayer nanotube (20 nm outer diameter) and (**b**) the corresponding diffraction pattern showing that the nanotube contains a majority of perpendicular or nearly perpendicular tubules; note the diffuse intensity between the equatorial (0002l) spots and the modulated streaking of the hexagonal spots.

narrow, forward-scattering beam allows a better resolution of the (000±2) spots which are seen to be elongated towards and away from the center of the pattern in Figure 3b. This micrograph and higher resolution ED micrographs (Bernaerts *et al.*, 1995a) indicate that the diffuse radial intensity can be resolved into weak, regularly spaced spots.

This phenomenon arises from an interference between the electron waves scattered by the left and right sides of the nanotube acting as parallel slits and therefore provides an implementation of the famous Young two-slits experiment performed here with electrons and a nanotube (a similar phenomenon was observed from intergrown lamellae in $Nd_{1-x}Ce_xCuO_4$ superconductor, Verwerft *et al.*, 1990). The theory developed later will provide the mathematical form of the diffuse intensity oscillations between the (0002m) spots. The first order circle in Figure 3b reveals several hexagonal sets of split spots due to perpendicular or nearly perpendicular tubules (of which the chiral angle, in the convention of Figure 2a, is about 27.5°, i.e., 2.5° away from the purely perpendicular configuration). The streaks are clearly observed to have a modulated intensity fading away from the axis.

The spots have varying contrast when tilting the nanotube axis away from the normal to the electron beam, as shown in the series of ED patterns of Figure 4. The intensity of the streaking is also changed by such tilting experiments. A detailed interpretation of these pictures has been provided by Zhang *et al.* (1993a,b) in terms of geometrical considerations in the reciprocal space of a cylindrical graphene sheet. The reader is referred to this reference for a complete discussion.

We now provide a different but qualitatively equivalent interpretation of the streaking phenomenon by reasoning in the real space of the nanotube (see also Amelinckx *et al.*, 1995a). A mathematical theory of streaking in the kinematical approximation will be given in the next section. When the electron beam travels towards a nanotube, it sees the honeycomb lattice of the graphene sheets of each tubule as having a well defined and constant lattice spacing along the tubule axis. However, it sees a shrinking lattice parameter along the tubule circumference, towards the tubule edges where the hexagons are looked upon at grazing incidence. The diffraction of the electrons will then give rise to spots which remain sharp in the direction along the tubule axis; but normal to it, the spots will be elongated away from the tubule axis, that is towards larger diffraction angles since produced by apparently shorter lattice spacings. The intensity of each spot increases towards the axis and ends up at the nominal hexagonal position. This behavior arises by virtue of the fact that the orientation of the honeycomb lattice perpendicular to the beam represents an extremum. According to the simplified view presented here, the streaking is the analogue, in wavevector space, of what is known, in the frequency domain, as "chirping" and is the reciprocal of the real-space apparent chirping of the lattice spacing around the tubule circumference. This concept can be spectacularly illustrated by optical simulation experiments, as explained in detail by Amelinckx *et al.* (1995a). It will be confirmed by the theory that the streak intensity does not vary continuously as predicted by this simple model but is modulated as a result of the same interference of the diffraction by the two tubule walls, as was invoked for the (0002m) spots.

The changes of the diffraction pattern upon tilting in Figure 4 are also a chirping phenomenon of sort but this time in the direction along the nanotube axis. Indeed, tilting the nanotube away from the normal to the beam reduces the apparent honeycomb lattice spacing along the tube axis as seen by the electron waves. Hence, while the (0002m) spots (which lie on the tilt axis) remain unaffected by the tilting, all spots not on the tilt axis must recede from it. This is clearly demonstrated in Figure 4 where the two pairs of spots marked A, B and C, D are seen to "climb up" the second order circle and end up coalescing at the top and disappearing when the tilt angle increases. Detailed geometrical constructions which explain the changes of the diffraction pattern upon tilting are discussed by Zhang *et al.* (1993b). The theory described below will allow us to perform computer simulations of the diffraction of a tubule by an off-normal electron beam. A practical use of

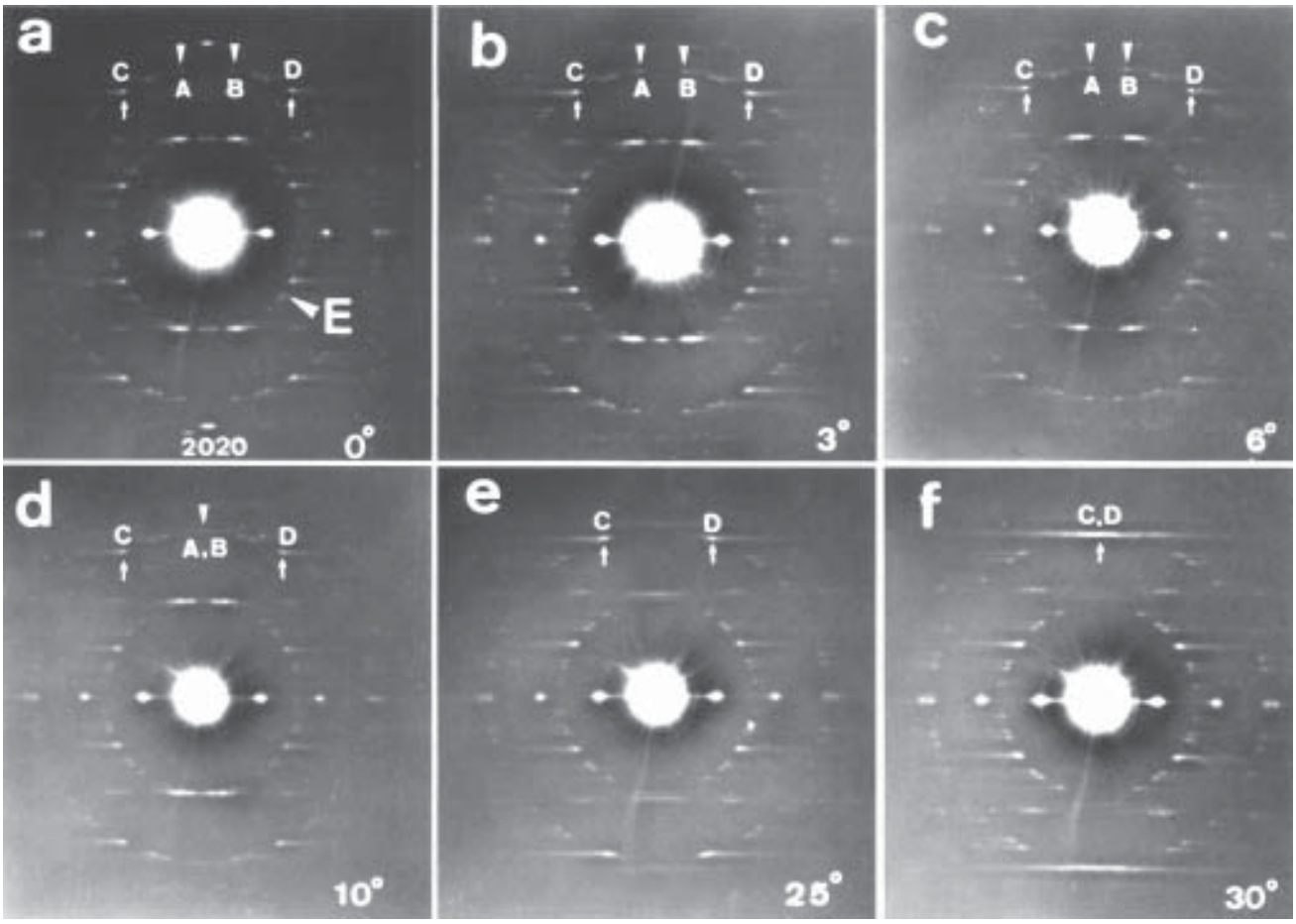

Figure 4. Sequence of electron diffraction patterns of a nanotube (18 layers with an innermost diameter of about 1.3 nm) obtained by tilting the vertical nanotube by the indicated angle about a horizontal axis. Note the changes in the spot contrast and in the streaking intensities. The second order symmetric pairs of spots marked A, B and C, D move toward the twelve o'clock position upon tilting. The spots C, D belong to achiral, parallel tubules and merge in Fig.4f when the tilt angle is 30°.

the tilting experiment will be discussed later.

Coiled nanotubes

When nanotubes are grown catalytically (Ivanov *et al.*, 1994), the inhomogeneity and anisotropy of the growth process on the surface of the supporting metal particle creates stresses in the nascent nanotube which may cause it to bend and twist periodically, resulting in the formation of a regular helix (Kawaguchi *et al.*,1992; Amelinckx *et al.*, 1994; Fonseca *et al.*, 1995). TEM images of such coils are shown in Figure 5. Consideration of the stiffness of the C-C sp^2 bond indicates that it would be quite impossible to deform elastically a straight nanotube into such a highly contorted shape. In addition, an elastically deformed tube would not remain stable upon release of the stress. Plastic deformation must have taken place at or near the interface with the metal particle during growth.

High resolution imaging of selected areas of the coil (Bernaerts *et al.*, 1995a), such as the one shown in Figure 6, reveals that the coiled nanotube is actually sharply bent at a succession of knees joining two straight cylindrical segments. Apart from their short length, the latter have the same structure as the micron-long straight nanotubes of the previous section. The polygonized texture of the coiled nanotube is confirmed by the corresponding diffraction patterns. Selected area ED micrographs of two helix periods and one single period are shown in Figures 7b and 7d, respectively, alongside bright-field images of the nanotubes (Bernaerts *et al.*, 1995a). The diffraction spots of each straight segment lie on quasi-continuous circles which are reminiscent of a powder pattern of ordinary graphite. But the most conspicuous feature is the first order diffraction arc labeled (0002) in Figure 7b. This arc is produced by the (0002) spots of the successive straight nanotube segments. It reflects the changing orientation of

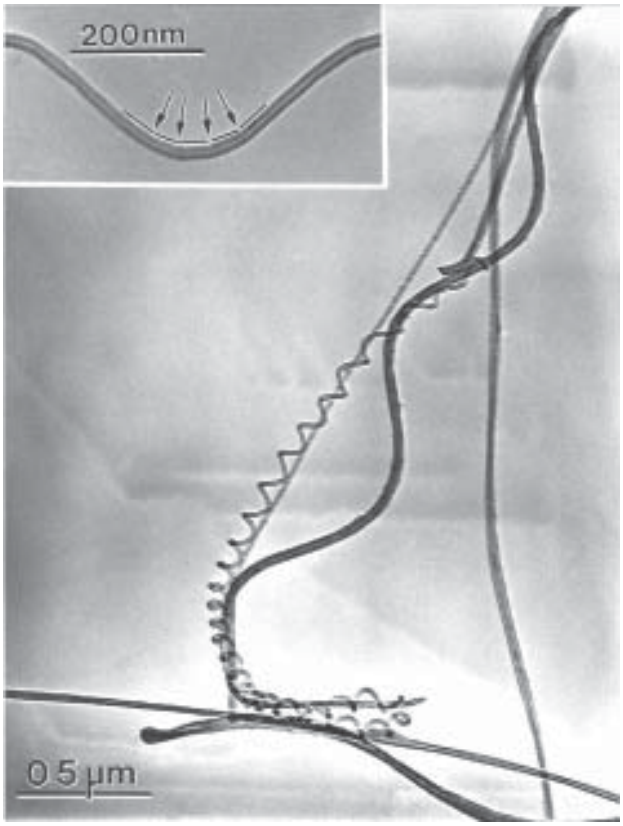

Figure 5. Coiled nanotubes of various radii and pitches. The inset indicates (arrows) than the coils are polygonized.

the segments of which the axis describes a cone around the helix axis. The angular opening of the arc is related to the helix radius-to-pitch ratio. Note in Figure 7d that the arc is spotty as a result of the "space quantization" of the segment orientation in the polygonized helix. Moreover, the arc is most intense at its edges, which again stems from the extremum nature of the segment orientation at the edges of the cone it describes. Counting the number of spots in the (0002) arc of Figure 7d or estimating the bend angle in Figure 6 indicates that there must be about a dozen straight segments per helix turn.

How can one connect two nanotube segments at an angle of about 30° without grossly distorting the honeycomb lattice of each of the graphene layers of the tubes? Remarkably, solutions to this problem were discussed theoretically by Dunlap (1992) and by Ihara *et al.* (1993) even before the observation of the coiled nanotubes. In Dunlap's construction, the bending of a single graphene tubule can be accomplished, while maintaining the continuity of the honeycomb lattice, by introducing a single pentagon at the apex and a single heptagon diametrically opposed at the saddle point of the knee. A ball-and-stick model of the structure is shown in Figure 8 (Fonseca *et al.*, 1995). Chiral as well as achiral tubules of equal or of different diameters can be connected in this way with just a single pair of 5-7 ring defects. In a multilayer coiled nanotube, the 5-7 rings of the knees in each layer are assumed to be aligned in a common direction (Fonseca *et al.*, 1995). Note that one or several atoms around the 5 and/or the 7 rings can be removed without causing the collapse of the knee which is kept rigid by the rest of the continuous honey-comb lattice. Hence, vacancies and vacancy clusters may have been inserted during the growth process in place of the highly strained, 5-7 topological defects.

The precise value of the knee angle is still a matter of discussions. A recent study by Zhang and Zhang (1995) using TEM and ED from a coiled nanotube seen along its axis reveals that there are just 12 straight segments per helix period in their particular sample and hence that the bend angle must be less than 30°. This appears to be consistent with Dunlap's estimation of 30° from his construction (Dunlap, 1994). However molecular model building (Fonseca *et al.*, 1995) as well as theoretical equilibrium structure calculations (Lambin *et al.*, 1995) suggest that the bend angle should be larger than or close to 36°, at least in the small diameter tubules which are amenable to such simulations. Note that bending at less than 36° can be accomplished by a non diametrically opposed 5-7 pair (Ihara *et al.*, 1993). High resolution TEM and ED observations specifically designed to study the knee region could lead to the identification of the actual or most frequently occurring modes of bending in coiled nanotubes.

Sequencing the nanotube chirality

We have discussed the effect introduced by the chirality of individual tubules on the diffraction pattern: each chiral tubule produces a pair of hexagons of streaking spots (in every diffraction order) whose angular separation, which is twice the chiral angle, can be measured accurately. But a complete characterization of a given multilayer nanotube would require the "sequencing" of the nanotube chirality, that is the specification of the chiral angle of each and every successive tubule of the nanotube. This remarkable feat appears to be within reach of high resolution electron microscopy by at least two different but related methods, one working in real space, the other via reciprocal space. The principle of both methods is illustrated in Figure 9.

The first method would involve an examination of the nanotube bright field image at the best resolution attainable today which allows one to resolve the graphene repeat distance of 0.21 nm between zigzag rows of atoms (Zhang *et al.*, 1993a). Consider, in the image of Figure 1a, one of the lattice fringes corresponding to the edge of a particular tubule whose chirality is to be determined. The method would consist in tilting the nanotube axis away from the normal to the electron beam until the zigzag (curved) "rows" at the edge of the chosen tubule are brought into alignment with the electron beam. A sketch of the tilting experiment is given in Figure 9a,b. When correctly aligned in this way, the quasi-continuous lattice fringe chosen

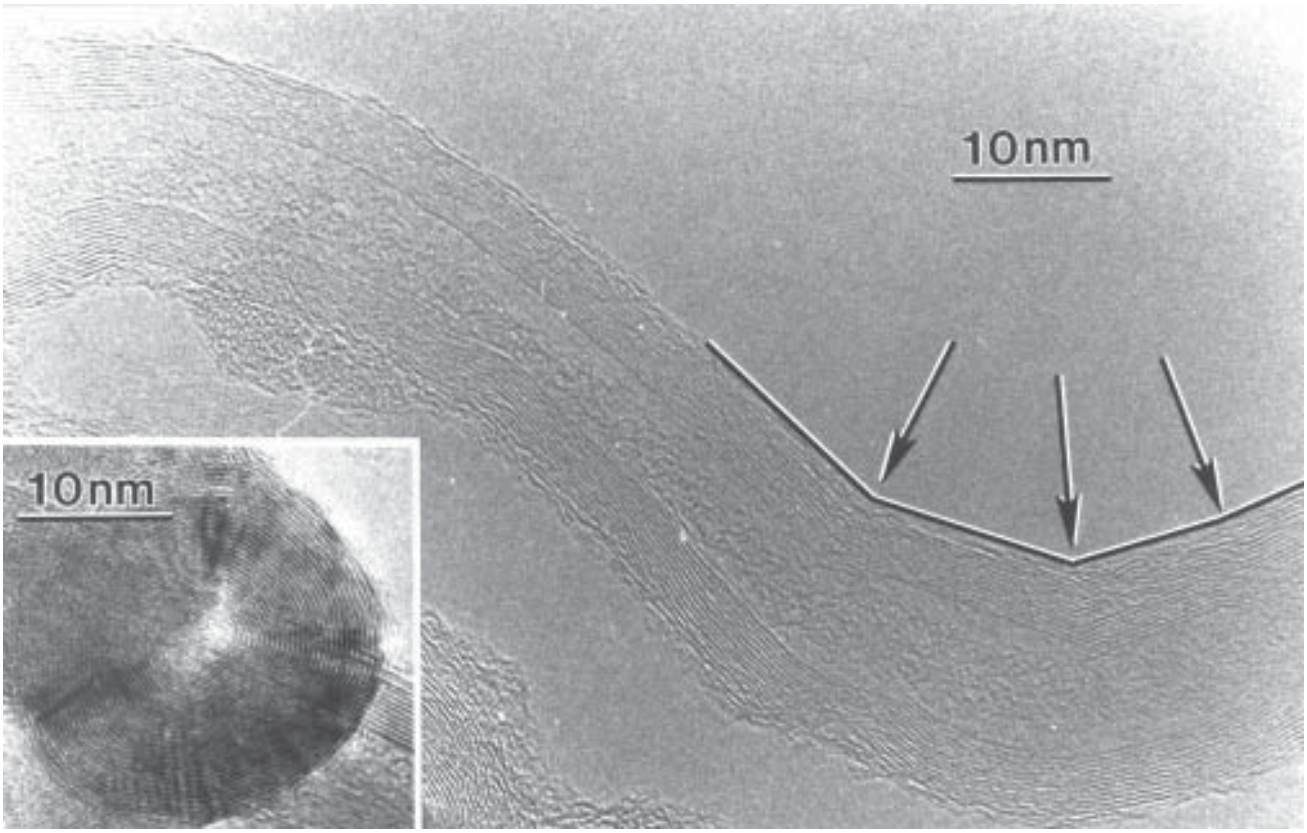

Figure 6. High resolution image of a coiled nanotube revealing its polygonized texture. The maximum projection of the polygon angle is about 30°. The inset shows the approximately circular cross section of the nanotube.

on the left side of the tubule in Figure 1a (or on the right side, depending on the chiral handedness) should break up into resolvable beads separated by 0.21 nm (Fig. 9b). The tilt angle and its sign would then give the chiral angle and handedness of that particular tubule. The method was already used in TEM of biological structures such as the helical arrangement of proteins in the tobacco mosaic virus (Finch, 1972, and references therein) and is also reminiscent of a computer experiment in which a space-filling model of a DNA molecule is tilted in order to obtain a better view through the small and large grooves of the double helix (Rich, 1992). A computer simulation (Bernaerts *et al.*, 1996) has demonstrated the feasibility in principle of this method. However, several practical problems, the most serious of which is the severe radiation damage caused by the high intensity electron beam in high-resolution TEM, have so far prevented the actual implementation of this direct approach.

The second method makes use of the diffraction contrast, dark-field imaging technique. It consists in producing an image of the nanotube by selecting, with a small objective aperture, those electrons which have been scattered into a particular diffraction spot belonging to one hexagonal set of chosen chiral angle. Such electrons will image primarily those tubules which are responsible for their diffraction into the selected spot and hence will allow, in principle, a "reading" of the position (relative to the bright field image of the nano-tube) of the tubule(s) having the chosen chirality. Among the spots belonging to a chiral tubule, the most suitable ones for dark-field imaging are those closest to the twelve o'clock (and six o'clock) site in the first order diffraction circle (Fig. 9c). As was discussed before, a tilting of the tubule axis away from the normal to the electron beam will cause these spots to climb towards the top (and bottom) of the diffraction circle and merge when the tilt angle coincides with the chiral angle of the tubule(s) under scrutiny. This is immediately clear by referring to Figure 9b again: for the correct chiral alignment, the zigzag atomic helices (drawn as continuous lines in Fig. 9) project into cycloids which have sharp horizontal cusps on the left (or right) side of the tilted tubule. The regular cusps generate a linear grating in the direction of the tubule axis which diffracts the electron waves and give rise to the two merging streaked spots at twelve o'clock, as discussed in the

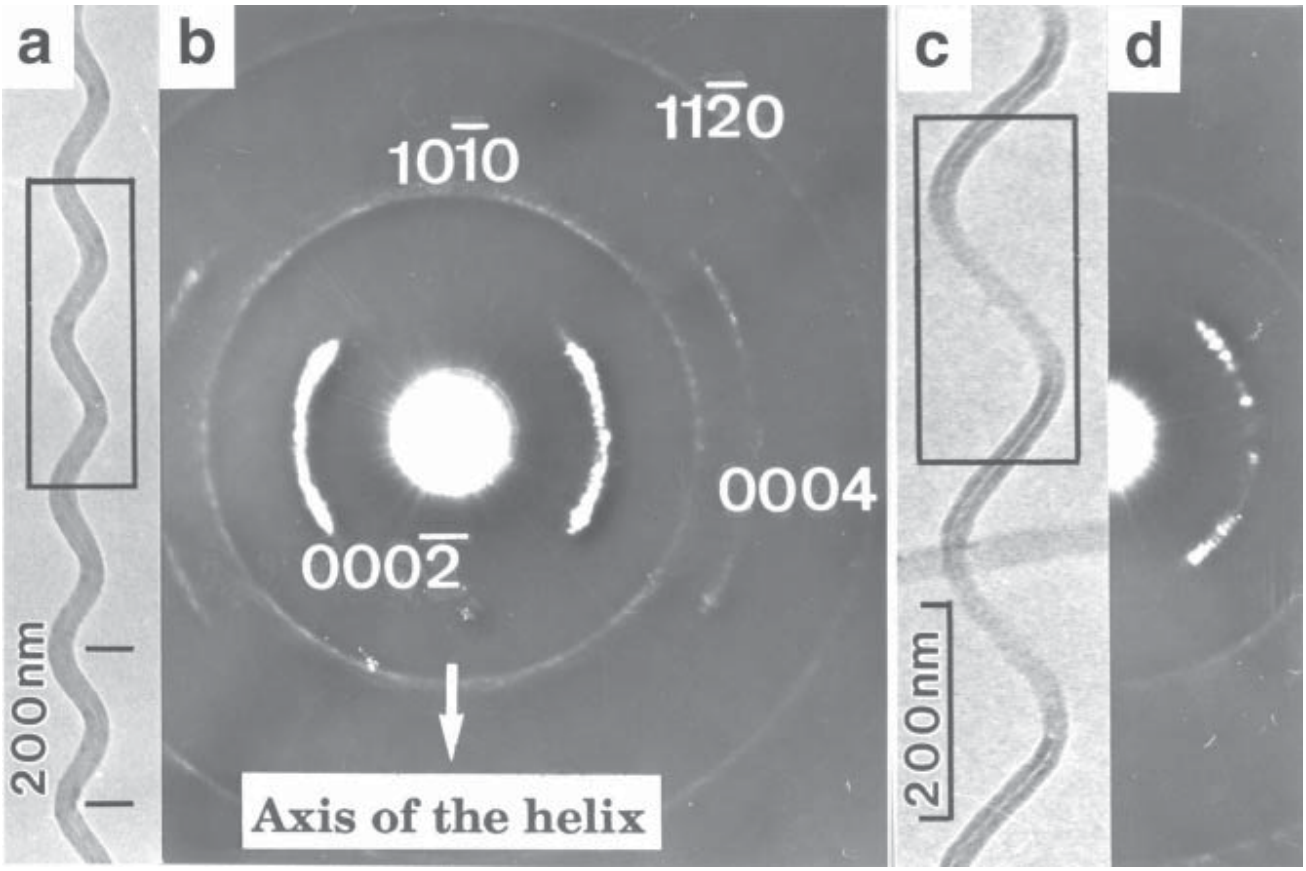

Figure 7 (**a**) Coiled nanotube and (**b**) the corresponding diffraction pattern of a selected area indicated in (a) by the rectangle and comprising two helix periods; note the (0002) arcs. (**c**) The same coiled nanotube as in (a) and (**d**) diffraction from a selected area of one single period; note the spotty appearance of the (0002) arc and the intensity maxima at the arc extremities.

previous section. Hence a small aperture placed there (Fig. 9c) will lead to a dark-field image illuminating a narrow portion of the left wall of the nanotube preferentially to the right wall (or vice-versa).

Very recently, Bernaerts *et al.* (1996) have given a first successful implementation of the dark-field imaging method. They produced a "map" of the chirality distribution in a multilayer nanotube and gave a detailed, reciprocal-space interpretation of the successful method. They further report on other remarkable observations in diffraction contrast, dark-field imaging bearing on the defective structures of nanotubes (Bernaerts *et al.*, 1996, 1997).

Kinematical Diffraction Theory

Validity of the First Born Approximation

In this section, we construct a kinematical theory of wave diffraction by a straight nanotube, in view of confirming the previous interpretations which were based on geometrical considerations alone. The theory will go beyond the geometrical description by allowing one to predict, under legitimate conditions, the relative diffraction intensities. This should be useful for X-ray diffraction (XRD) for which, as is well known, the kinematical theory is generally adequate. Unfortunately, there are so far very few XRD studies of carbon nanotubes. One early measurement on a nanotube powder is due to Zhou *et al.* (1994) and the theory presented here should prove useful for interpreting the observed θ-2θ plot. Ideally, one would like to experiment on a single crystal or, at least, on oriented nanotube fibers. Macroscopic samples of oriented nanotubes have been successfully prepared for other purposes (de Heer *et al.*, 1995), but these samples are not likely to be made of nanotubes of a single species (e.g., monodispersed diameter, unique chirality distribution) as one would like to have for exploiting an XRD fiber diagram (see however the very recent paper by Thess *et al.*, 1996).

The definite advantage of electron diffraction over

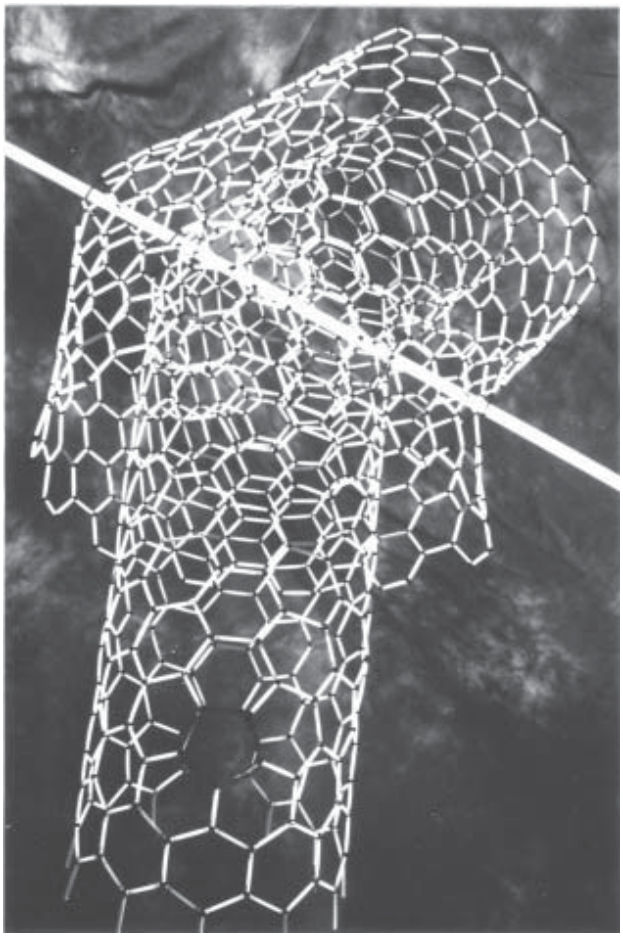

Figure 8. Ball-and-stick model of a single nanotube knee of about 30°. The bend is obtained by inserting a pair of pentagonal and heptagonal ring defects diametrically opposed at the outer elliptic and inner hyperbolic (saddle) points of the knee. The stick connects the aligned 5-7 rings in the two tubules which are separated by the 0.34 nm graphitic distance.

XRD is that the scattering power of atoms for electrons is such that the beam can be focused onto one single nanotube for diffraction and imaging, as illustrated in the previous section. This very advantage however usually entails one interpretational drawback, namely that the conditions for the validity of the first Born or kinematical approximation to describe the electron scattering quantitatively may be difficult to meet (Gevers, 1970): for heavy materials, the applicability of the kinematical theory to the calculation of Bragg spot intensities demands that the thickness of the diffracting object traversed by the electron beam be less that 10 nm. For carbon nanotubes however, the conditions should not be so severe on account of the smaller scattering power of the light carbon atom, as we now show.

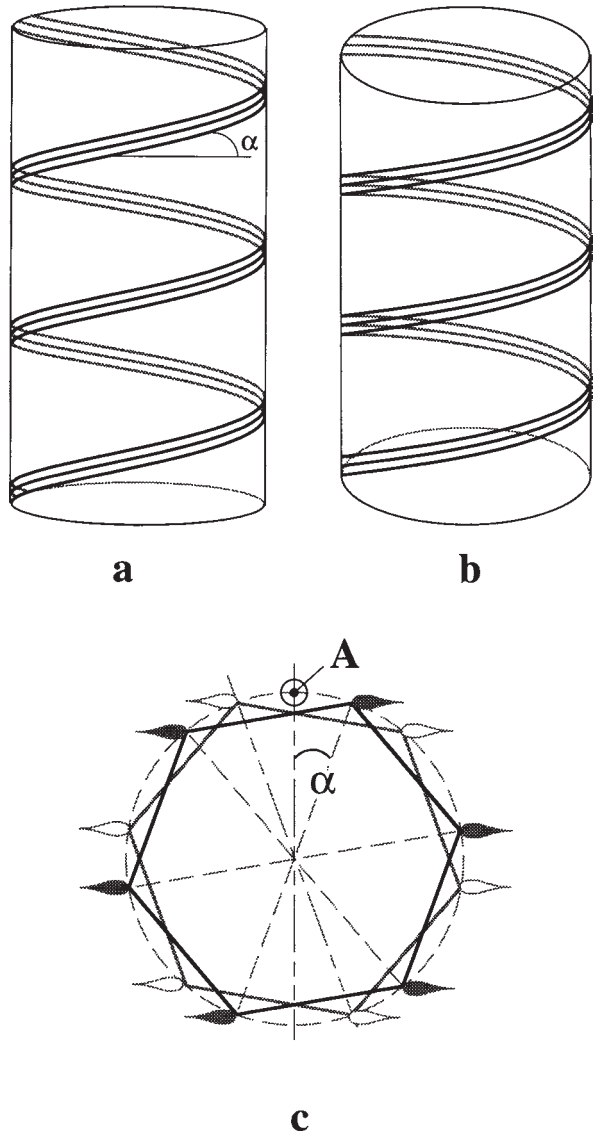

Figure 9. Principle of the tilting experiment to determine the handedness of a chiral tubule. In (**a**) a familly of three zig-zag rows of atoms are represented as parallel, right handed spirals making an angle a with the horizontal, tilting axis. In (**b**) the tubule axis has been tilted by an angle α, its upper tip toward the viewer; note that the sinusoidal projections of the spirals in (a) have changed to cycloids in (b) with their sharp cusps appearing on the left side of the tubule. In (**c**) the streaked spots at one and eleven o'clock move upon tilting toward the twelve o'clock position marked **A** where an aperture is placed for dark-field imaging of the tubule.

The kinematic atomic scattering amplitudes $f_e(\mathbf{q})$ of elements for fast electrons have been compiled by Smith and Burge (1962) and by Doyle and Turner (1968) who analyzed

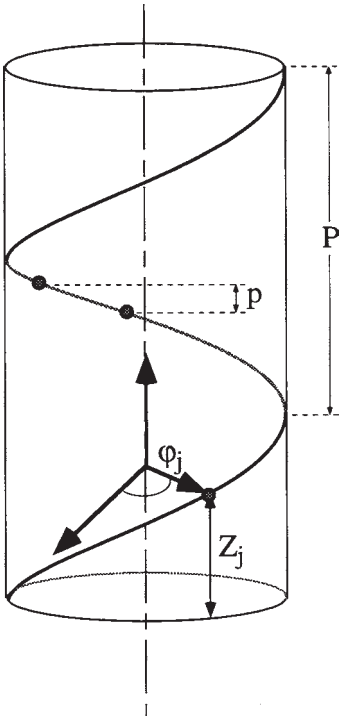

Figure 10. Cylindrical coordinates of atoms on a regular circular helix of pitch P and atomic repeat distance p along the helix axis.

scattering factors calculated from realistic atomic wavefunctions. The first Born approximation to high-energy electron scattering (by the screened nuclear Coulomb potential) used in these calculations is dominant provided that the "fine structure constant" $Ze^2/\hbar v = (Zc/v)/137$, where Z is the nuclear charge and v is the electron velocity, is much smaller than one (Landau and Lifshitz, 1967). For Z = 6 and for 300 keV electrons, a typical electron energy used in the TEM-ED works discussed in the present paper, one finds $Ze^2/\hbar v \approx 0.07$, a value indeed small enough to validate the first Born approximation. From the tabulated data (Doyle and Turner, 1968), one can then estimate a total elastic cross section (including the correction of relativistic length contraction) of σ Å $2.2\ 10^{-2}$ Å^2 per carbon atom. Ignoring coherent scattering within and between the graphene layers, of which the area density is about 0.4 atom/Å^2, we find that the total scattering probability is of order 10^{-2} per atomic layer. After traveling through N layers, the relative Poisson probabilities for single and double scattering would be 10^{-2}N and 10^{-4}N^2/2! respectively. If we demand that the double scattering be less than 10 % of the single scattering, N may not exceed 20 layers.

In a quantitative evaluation of the intensity of electron wave diffraction by a crystalline, cartesian material, one eventually considers the "extinction distances" ξ_g for Bragg beams characterized by the reciprocal lattice vectors **g.** In the so-called one-beam kinematical theory (Gevers, 1970), ξ_g is the distance traveled after which the wave intensity is totally transferred by elastic scattering from the forward beam to the diffracted beam **g** in the exact Bragg orientation. For the kinematical theory to be valid, the thickness traversed by the beam should be much smaller than all ξ_g. For electrons of kinetic energy E and wavelength λ, ξ_g at the exact Bragg angle is given by ξ_g Å $\lambda E/V_g$ where V_g is the corresponding Fourier component of the atomic lattice potential for the high-energy electrons. V_g is related to the atomic scattering amplitude $f_e(\mathbf{g})$ by

$$Vg = \frac{1}{\Omega}\left(\sum_{\mu} e^{ig.a_{\mu}}\right)\frac{\hbar^2}{2m} f_e(g)$$

where the Σ_μ extends over the independent atomic sites $\mathbf{a}_\mu$ in the graphite unit cell of volume Ω Å 17 Å^3. Using again the table of $f_e(\mathbf{g})$ in Doyle and Turner (1968), one finds V_g Å 0.25 eV for the lowest-order **g** parallel to the graphene plane. Due to such a relatively small value of the carbon crystal potential, for E = 300 keV one finds ξ_g Å 2.5 μm or about 7000 graphite layers. Hence, in bulk graphite, the forward beam in an exact Bragg direction will not be appreciably depleted by elastic scattering until traversing several hundred layers. For directions away from an exact Bragg angle, the depletion by each of the diffracted beams is much reduced (Gevers, 1970). In nanotubes, the turbostratic disorder of successive tubules will tend to suppress the coherent Bragg scattering and prevents the build up of amplitude in particular reflections.

We thus reach the conclusion that the kinematical theory should be a valid approximation for carbon nanotubes made of several tens of monolayers and hence the theory appears to be quite suitable for the nanotubes actually observed in the works reported above.

CCV Theory

In formulating our theory, we take the view that a straight monolayer tubule can be constructed by assembling a finite set of parallel monoatomic carbon helices sharing the nanotube axis. A glance at Figure 2 shows that this can be done in a number of ways both for achiral and for chiral tubules. We use this approach because there already exists an analytical treatment of diffraction by a regular, monoatomic, circular helix. The theory was developed by Cochran, Crick and Vand in 1952 (Cochran *et al.*, 1952, referred to here as the CCV theory) for the diffraction of X-rays by polypeptide α-helices and was applied to DNA molecules shortly thereafter (Watson and Crick, 1953; Franklin and Gosling, 1953. See also Klug *et al.*, 1958; Vainshtein, 1966). These biological molecules often can be viewed as collections of C, H, N, O, P, S etc. coaxial helices. The CCV theory turns out to be particularly

straight-forward to apply to straight, circular carbon nanotubes since they have a single type of atoms regularly arranged along exactly circular and equidistant coaxial helices. The theoretical approach developed here is similar to the one introduced earlier by Qin (1994) and was formulated quite independently (Lucas *et al.*, 1996).

To set the notations, we provide a particularly straightforward derivation of the CCV result. The scattering amplitude of a collection of atoms at fixed positions $\mathbf{r}_j$, is given by

$$T(k) = f(k)A(k) \equiv f(k)\sum_j e^{ik.r_j} \tag{1}$$

where **k** is the wavevector transfer and f(k) is the kinematic atomic scattering factor for X-rays or for electrons, assumed to be isotropic (the theory can be generalized to "anisotropic" atoms). The diffraction factor A(**k**) is the Fourier transform of the nuclei density

$$p(r) = \sum_j \delta(r - R_j)$$

On a regular, circular, monoatomic helix of radius r, pitch P and atomic repeat distance p in the z-direction of the helix axis, the atomic positions are given, in cylindrical coordinates, by (see Fig. 10)

$$r_j = \left(r, \phi_j = \frac{2\pi}{P} z_j, z_j = jp + z_o \right) \tag{2}$$

where j is an integer and (r, ϕ_o, z_o) are the coordinates of an atom taken as a conventional origin. To evaluate equation (1) in cylindrical coordinates according to equation (2), we use the Jacobi-Anger expansion of a plane wave in Bessel functions (Arfken, 1985):

$$r_j = \left(r, \phi_j = \frac{2\pi}{P} z_j, z_j = jp + z_o \right) \tag{3}$$

where

$$k \perp = \sqrt{k_x^2 + k_y^2}, \psi_k = \tan^{-1}\left(\frac{k_y}{k_x}\right)$$

and **k** = (k_x,k_y,k_z) are the cartesian coordinates of the wavevector transfer. This relation can be readily demonstrated by noting that the plane wave, being a periodic function of φ, can be expanded in the Fourier series (eqn. 3) of exp(-inφ); the expansion coefficients are obtained, in the usual way, as an integral of the left hand side of equation (3) multiplied by exp(inφ), which yields the Bessel function J_n and the other phase factors in equation (3). Substituting equations (3) and (2) into equation (1), the summation over j in (1) can then be performed by using the well known identity

$$\sum_j e^{i\left(k_z p - 2\pi n \frac{p}{p}\right) j} = \sum_m \delta\left[k_z - 2\pi\left(\frac{\pi}{P} + \frac{m}{p} \right) \right] \tag{4}$$

The result is the CCV formula:

$$T(k) = f(k)\sum_{n,m} \delta\left[k_z - 2\pi\left(\frac{n}{P} + \frac{m}{p} \right) \right] \times e^{in\left(\psi_k + \frac{\pi}{2}\right)} J_n(k \perp r) e^{-in\phi_o + ik_z z_o} \tag{5}$$

The diffracted intensity is the square modulus of this expression. The δ-function means that the intensity is nonzero only on horizontal "layer-lines" [Polanyi (1921): the basic concept of layer-planes and layer-lines in the X-ray structures of fibers is implicit in this paper. The word "layer-line" (Schichtlinie) first appears in this paper and has been used ever since to describe X-Ray fiber diagrams). The layer-lines are positioned at

$$k_z = 2\pi\left(\frac{n}{P} + \frac{m}{p} \right) \equiv 2\pi \frac{1}{T} \tag{6}$$

If P/p is irrational, k_z can take all real values. If P/p is rational the layer-lines occur only at discrete values of k_z = 2πl/T where l is an integer and T, the true helix period, is the smallest common multiple of P and p.

We can now apply this result to a nanotube.

As Figure 2 illustrates, a tubule of arbitrary chirality can conveniently be specified by two integers (L,M) giving the position of the hexagonal atomic cell which, on rolling up a flat sheet of graphene to make a seamless tubule, is brought in coincidence with the cell at the origin (Hamada *et al.*, 1992). Parallel and perpendicular achiral tubules are of the type (L,0) and (M,M), respectively. Let us arbitrarilly choose in Figure 2a one of the zig-zag rows of atoms which makes a nonzero angle with respect to the tubule circumference C. In Figures 2b, c or d, these atoms make two helices related to one another by a single screw operation (z_1, φ_1). Shifting this zig-zag pair of helices L 1 times by the tubule helical symmetry operation (z_o, φ_o) covers the tubule completely (discussions of helical

symmetries of nano-tubes have been given by Klein *et al.*, 1993, White *et al.*, 1993, and Dresselhaus *et al.*, 1995). The diffraction amplitude of the complete tubule is therefore obtained by adding up the amplitudes, as given by equation (5), of a finite set of L helix pairs. Since the successive amplitudes differ only by phase factors, the total amplitude will involve summing a geometrical series.

Diffraction by an Achiral Tubule

As an illustration of how the method works mathematically, let us consider the simple case of a parallel tubule (L,0) (Fig. 2c). From equation (1), an initial zig-zag pair of helices separated by the pure translation (z_1=d,φ_1=0) along the z-axis will produce the scattering amplitude

$$A_{pair}(k) = \left(\sum_j e^{ik.R_j}\right)\left(1 + e^{ik_z z_1}\right) \tag{7}$$

where z_1 = d Å 0.14 nm is the C-C bond distance. Note in passing that the pair amplitude vanishes if $k_z z_1$ is an odd multiple of π. This happened to be the case for the celebrated B-DNA molecule (Franklin and Gosling, 1953) which has two helical strands displaced by z_1 = 3P/8 and of which the X-ray fiber diagram indeed shows a missing 4th layer-line ($k_z z_1 = 3\pi$).

If we now subject the pair of helices to L-1 pure translations (z_o=3d, φ_o=0) along the z-axis and add up the amplitudes (7) for each pair, the amplitude gets multiplied by the geometrical series

$$\sum_{n=0}^{L-1} e^{ink_z z_o}$$

The result is

$$A_{tub}(k) = \left(\sum_j e^{ik.R_j}\left(1 + e^{1k_z z_1}\right)\frac{1 - e^{iLK_z z_o}}{1 - e^{iK_z z_o}}\right. \tag{8}$$

The first factor is the amplitude of a single helix, as given in equation (5); the second means that there are two kinds of inequivalent helices in the tubule, just as there are two inequivalent atoms in the hexagonal unit cell of the honeycomb lattice; and the last factor gives the interference between all the pairs in the complete tubule. Because in a parallel tubule the helix period is P = Lz_o = 3dL and because k_z is quantized to the layer-lines k_z = 2πl/P, this last factor amounts to

$$\frac{1 - e^{iLk_z z_o}}{1 - e^{iK_z z_o}} = \frac{1 - e^{i2\pi l}}{1 - e^{i2\pi l/L}} = L\delta_{l,sL} \tag{9}$$

where the Kronecker $\delta_{l,sL}$ suppresses all layer-lines except those at l = sL, s integer. The diffraction pattern is therefore confined to layer-lines separated by integer multiples of 2πL/P = 2π/3d which is the expected result since, in the parallel tubule, the repeat distance in the z-direction is 3d. Along each allowed layer-line, the intensity is given by a linear combination of Bessel functions. As will be seen in the computer simulations, the overall result is a mm2-symmetric hexagonal set of spots streaking, in an oscillatory fashion, away from the tubule axis.

Diffraction by a Chiral Tubule

We now formulate the result of the application of the CCV theory to the diffraction amplitude of a general chiral tubule specified by the two arbitrary integers (L,M). The pattern is again organized in layer-lines labeled by an integer l. The total scattered amplitude along the l'th layer-line factorizes as follows:

$$T_{tub}(k) = f(k)\sum_n J_n(k \perp r)e^{in(\psi_k + \pi/2)} \tag{10}$$

$$A_n(L,M) \quad B_n(L,M)$$

The scattered intensity is the square modulus of this expression. The factors have the following meaning: f(k), J_n and ι_k have been defined before in equations (1) and (3); A_n(L,M), represents the contribution of the two inequivalent helices of the tubule, as in equation (8), and is given by

$$A_n(L,M) = 1 + e^{i(-n\phi_l + 2\pi l z_l/T)} \tag{11}$$

B_n(L,M) is the factor associated with the summation over L pairs of helices making up the complete tubule:

$$B_n(L,M) = \frac{1 - \exp\left[i\left(-n\phi_o + 2\pi l\, z_o/T\right)L\right]}{1 - \exp\left[i\left(-n\phi_o + 2\pi l\, z_o/T\right)\right]} \tag{12}$$

Let us denote by C the circumference of the tubule in units of the honeycomb lattice parameter d√3. This is given by

$$C = \frac{2\pi r}{d\sqrt{3}} = \sqrt{\left(L^2 + LM + M^2\right)} \tag{13}$$

The sum over n in equation (10) is restricted to integer values

of n satisfying the selection rule of the l'th layer-line

$$l = nq + mp \tag{14}$$

where m is an integer and p, q are integers obtained after reduction of the rational fraction

$$\frac{p}{q} = \frac{2C^2}{L + 2M} \tag{15}$$

Irrespective of the chirality, the true helix period T is always an integer multiple of the atomic period along the axis of a carbon helix and is given by (Dresselhaus *et al*., 1995):

$$T = p\frac{3L}{2C}d \tag{16}$$

Finally the screw operations (φ_o, z_o) and (φ_1, z_1) are obtained from

$$\phi_o = \frac{2L + M}{C^2}\pi, \tag{17}$$

$$z_o = \frac{-3M}{2C}d \tag{18}$$

These formulae are arrived at by simple geometrical constructions in the plane of the honeycomb lattice.

Then, taking equations (14)-(18) into account, some algebra shows that the factor in equation (12) simply reduces to

$$B_n = L\,\Sigma_s \delta_{n+mM,sL} \tag{19}$$

where s in any integer. The effect of the Kronecker δ-functions is to eliminate all layer-lines pertaining to the single, original helix pair and to leave only such layer-lines as will construct two hexagonal patterns of spots each rotated by the chiral angle ± α with respect to the mm2-symmetric position (i.e., the position characteristic of an achiral (L,0) tubule). Due to the oscillations of the Bessel functions, each "spot" is a streak fading away in an oscillatory fashion perpendicular to the meridional axis of the pattern.

Computer Simulations

We now illustrate the theory with computer simulations of the diffraction by straight tubules and nano-tubes. In the calculations, we have used the actual kinematic form factor for carbon such as listed by Doyle and Turner (1968). Since in electron microscopy work, the spot intensities are seldom measured quantitatively, our simulations will at this stage serve only to confirm the capability of the theory to obtain the qualitative features of the diffraction patterns.

We note that the complete formula in equations (10)-(12) is computationally extremely efficient: the only variable input is the pair of integers (L,M) which give the tubule size and chirality. The position of each layer-line of nonvanishing intensity is determined in advance by the purely geometrical factor $B_n(L,M)$; and along a given layer-line, the intensity calculation demands only a few dominant Bessel functions. Due to the closed form of the formula, the computing time is independent of tubule size. By contrast, the brute force calculation of the scattering from the thousands of individual atoms would require constructing their coordinates and sweeping the reciprocal space in search of the diffraction spots.

Monolayer tubules: normal incidence

In the spirit of our approach of building up a tubule by assembling a set of helices, we first present the result of a computer experiment: Figure 11 shows the successive patterns obtained by diffraction, at normal incidence, from an increasing number of helix pairs, beginning with just one pair (Figure 11a) and ending with the full complement of L=18 pairs of a complete (18,0) parallel tubule (Fig. 11d). In Figure 11a, one recognizes the diamond and maltese cross structures characteristic of the diffraction by a regular helical molecule such as the celebrated DNA (Franklin and Gossling, 1953). There are many layer-lines along which the intensity is given by a dominant Bessel function of increasing order. Note that the regions about the long diagonals of the diamonds are extinguished by the destructive interference between the waves scattered by the two inequivalent helices (in this simulation, the two inequivalent helices were chosen to be connected by parallel C-C bonds shown in the perspective drawing below the pattern; note that this choice of starting helix pair, which corresponds to the analytical formulae of equation 18, is different from the zig-zag pair discussed previously. The end result of the simulation for the complete tubule is of course independent of this choice). In the next three patterns produced by 6, 12 and 18 helix pairs, the layer-lines are seen to become progressively removed by destructive interferences, except for those destined to build up the final hexagonal, mm2 symmetry pattern.

The spots are elongated perpendicular to the tubule axis: this is the streaking phenomenon observed in the real ED patterns (Iijima, 1991; Iijima and Ichihashi, 1993; Zhang *et al*., 1993b). The intensity modulation of the zeroth layer-line is essentially a representation of the oscillations of the zeroth order Bessel function. This central line would be the only one present if the scattering pattern was produced by a smooth, continuous cylinder of the same radius. The oscillations basically represent a slit function and arise from the interference

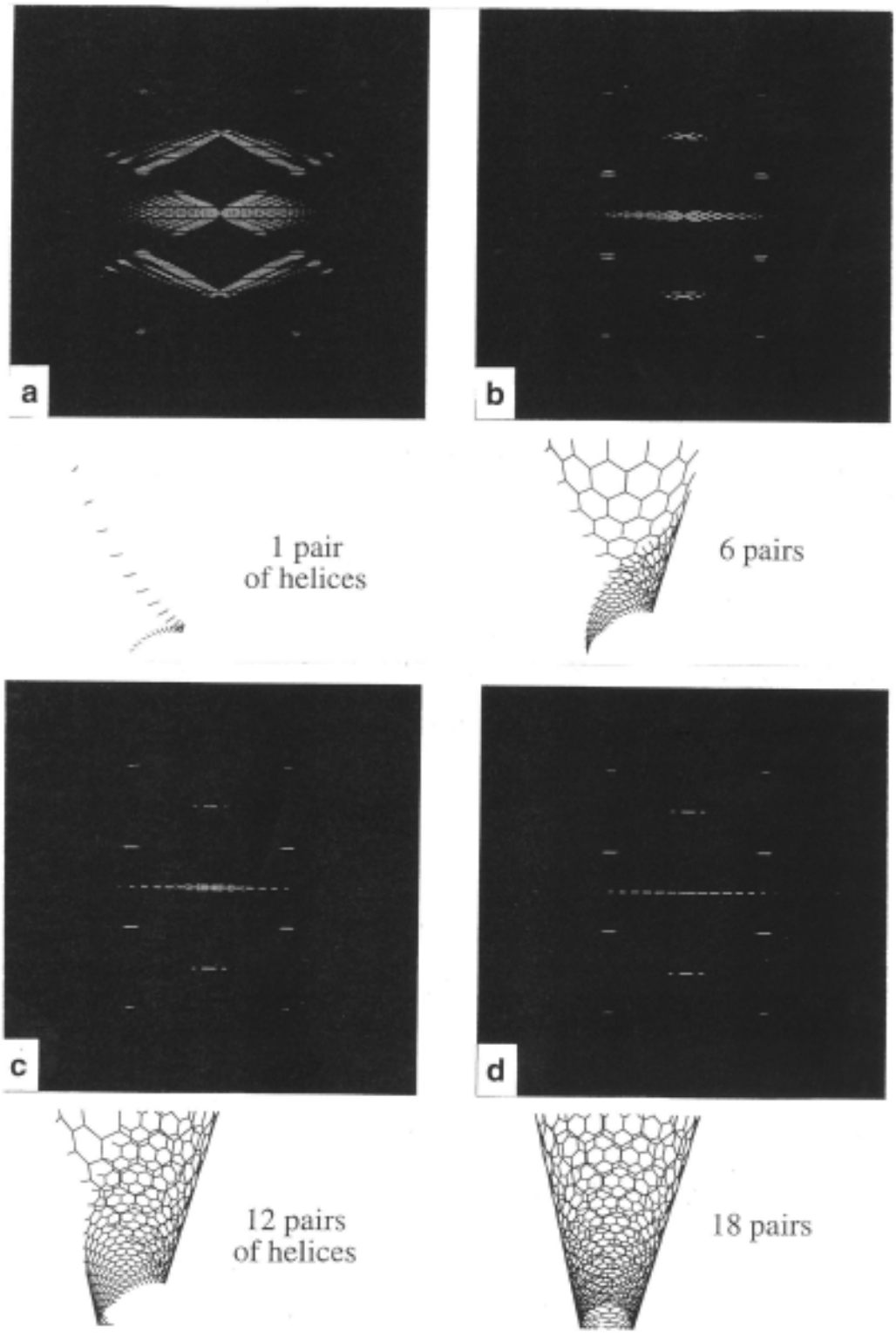

Figure 11. Computer simulations of the diffraction patterns of an increasing number of helix pairs from one pair (**a**) to the complete set of 18 pairs (**d**) making up the complete (18,0) tubule. The diamond repeat of the maltese cross characteristic of atomic helices in (**a**) is seen to evolve into the hexagonal spot pattern of a tubule in (**d**) by the destructive interference removal of intervening layer lines in (**b**) and (**d**).

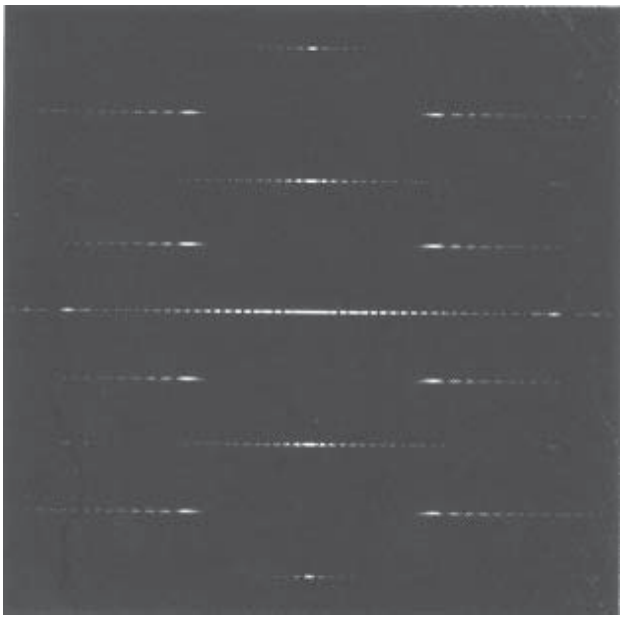

Figure 12. Computer simulation of the diffraction pattern of a (36,0) tubule. The modulation frequency of the streaks is doubled as compared to the case of the twice smaller (18,0) tubule in Figure 11d.

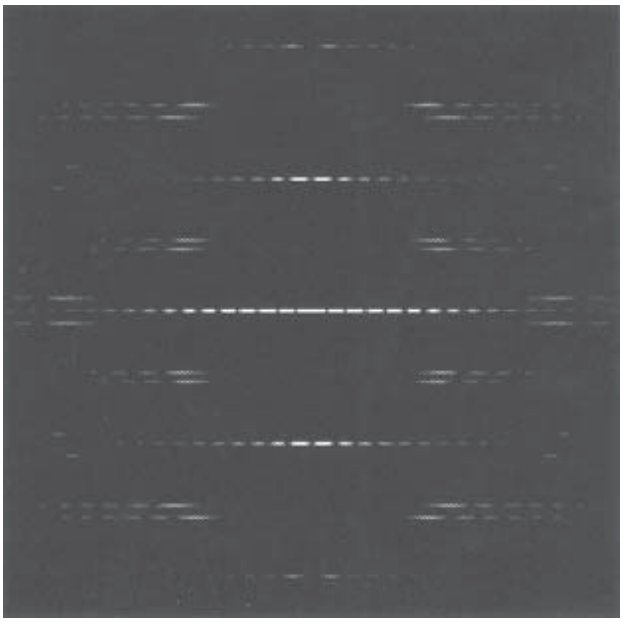

Figure 13. Computer simulation of the diffraction pattern of an (18,1), nearly parallel, chiral tubule. There are now two sets of hexagonal streaked spots turned with respect to each other by twice the chiral angle of 2.68°.

between waves scattered by the two edges of the cylinder. Such a continuous tube has only one characteristic length, its diameter, which sets the length scale for the argument of the Bessel function. This is further demonstrated by Figure 12 which is the normal incidence diffraction pattern of a (36,0) parallel tubule. The oscillation frequency in the zeroth layer-line has doubled in comparison with Figure 11d. The streaking spots now also exhibit intensity oscillations which reflect the same interference effect of the tubule edges. These streak modulations were barely visible in the less contrasted picture of the smaller (18,0) tubule. The enhanced contrast in the (36,0) pattern also reveals the second order hexagon of streaking spots. The present interpretation of the modulated streak intensities was already provided by Iijima and Ichihashi (1993) in terms of Fraunhofer diffraction from the two portions of the tubule parallel to the incident electron beam.

Figure 13 shows the simulated diffraction of an (18,1) chiral tubule. There are now two first order hexagonal sets of spots which are obtained from the achiral parallel hexagon of Figure 10d by clockwise and counterclockwise rotations by the small chiral angle $\cos^{-1}[(2L+M)/2C]$ Å 2.68°. Note that the twelve o'clock streak has split into two symmetric modulated streaks, leaving zero intensity on the (projection of the) tubule axis.

Although only the amplitudes are additive and not the intensities, one expects that the general geometrical features in the diffraction pattern of a multilayer nanotube will reflect the patterns of individual tubules such as shown in Figures 12 and 13. Since the chiral angle can vary from zero (parallel tubule) to 30° (perpendicular tubule), a nanotube will usually contain a number of tubules with small chiral angles, say of the order of or smaller than 10°. Such tubules will produce overlapping horizontal streaking spots near the twelve o'clock (and six o'clock) positions, because the streaking is nearly tangent to the first order circle around these positions. Due to the finite resolution in the ED micrograph, this overlap will therefore result in thick and long streaks about one and 11 o'clock. The other four hexagonal spots of each tubule however will give rise to well resolved pairs of nonoverlapping streaks, as in Figure 13. This explains the frequently observed reinforced streaks at the top and bottom of the first order diffraction circle, such as those shown in Figures 1b and 4. For a nanotube containing a majority of nearly perpendicular tubules, the horizontal streak reinforcement should appear at twelve o'clock in the second-order circle, as in Figure 3b.

Monolayer tubules: oblique incidence

We have performed calculations of the diffraction of an electron beam by a tubule at various incidence angles, in order to simulate a tilting experiment such as the one shown in Figure 4. A large (25,10) tubule of 2.41 nm diameter and 16° chiral angle was selected for the simulation. The four diffraction patterns in Figure 14 correspond to tilting the tubule

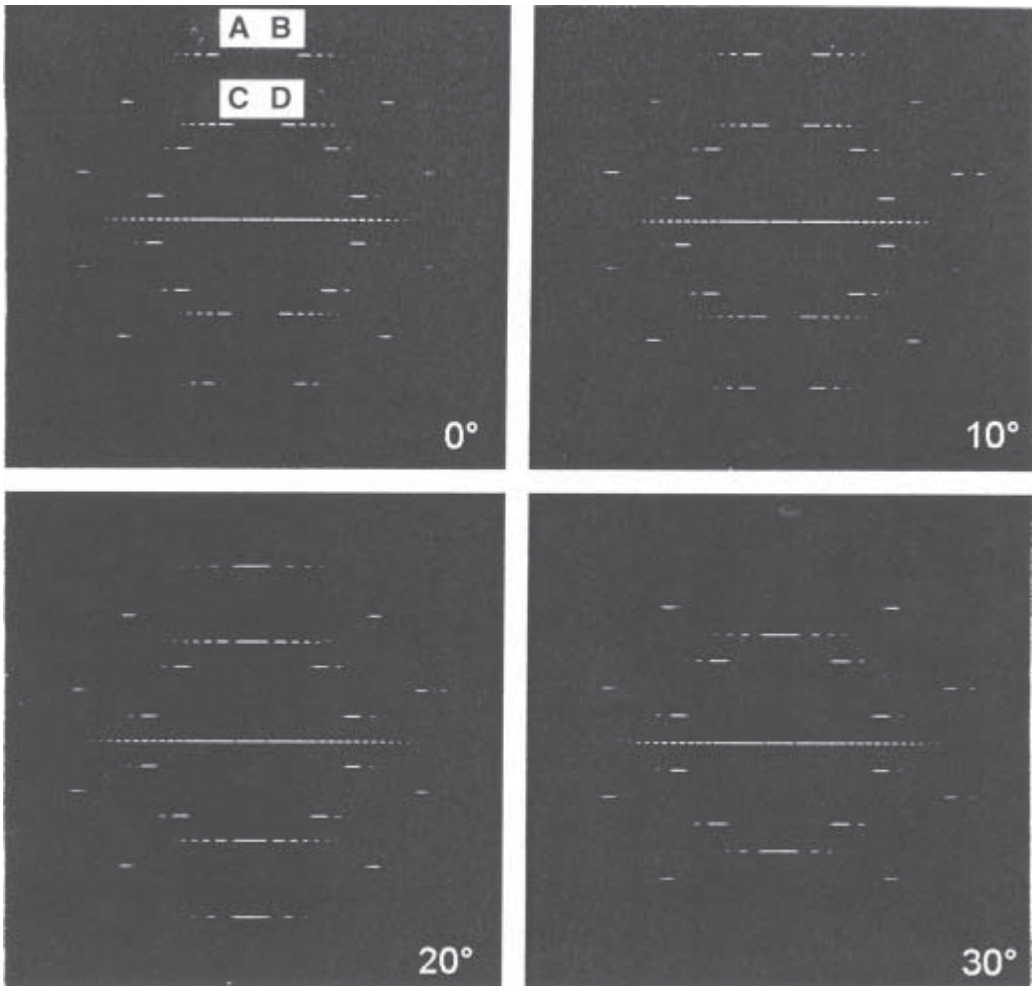

Figure 14. Computer simulation of the diffraction patterns obtained by tilting the axis of a (25,10) tubule through the indicated angles. This computer experiment simulates qualitatively the real experiment shown on Figure 4. Note the motion of the spots A, B and C, D upon tilting.

axis away from the beam normal by an angle θ of 0, 10, 20 and 30 degrees, respectively. The detailed effect of tilting the sample can be computed from Eqn. (10) by rotating the transfer wavevector **k** by an angle θ around the y-axis in the opposite direction.

One observes that the layer-lines recede from the zeroth order layer-line when θ increases. Measuring distances between layer-lines in the direction of the tubule axis confirms that they increase like $1/\cos\theta$. This "chirping" in reciprocal space corresponds to a decrease of the apparent axial lattice spacing, as seen by the electron waves, by a factor $\cos\theta$ (this is easily verified by considering a simple line grating at oblique incidence, see Amelinckx *et al.*, 1995a). The other striking effect of the tilting on the diffraction pattern is the "climbing motion" of the pair of spots marked A,B and C,D towards the twelve o'clock position on their respective circles. They form a single streak when $\theta = 20°$ and beyond but the simulation shows that they began to coalesce when θ neared the chiral angle of 16°. This behavior reproduces qualitatively the observation of Figure 4. It justifies setting the dark-field imaging aperture at twelve o'clock to measure the chiral angle of a tubule or set of tubules, as discussed previously (Fig. 9c).

Multilayer Nanotubes

A nanotube containing N coaxial tubules separated by the graphite interlayer spacing c_o Å 0.34 nm is fully specified by giving i) a set of integer pairs (L_m,M_m), m = 1,...,N, specifying the chirality sequence and ii) the relative registry between the successive tubules, i.e. the cylindrical coordinates $(r_m,\varphi_{om},z_{om})$

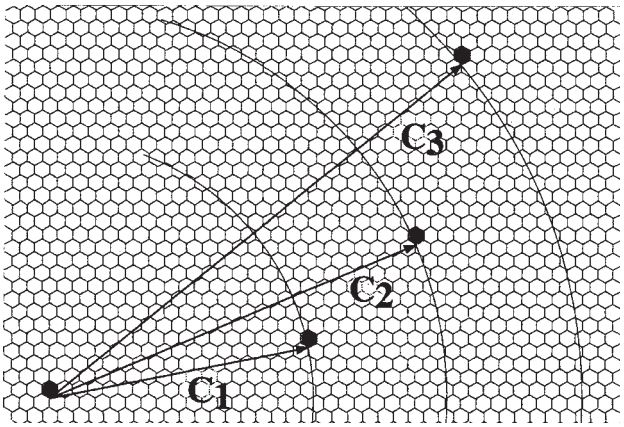

Figure 15. Construction in the graphene lattice of tubule circumferences for coaxial tubules separated by the graphitic distance of 0.34 nm. All lattice points sitting on or near the circles define possible tubules for a multilayer nanotube.

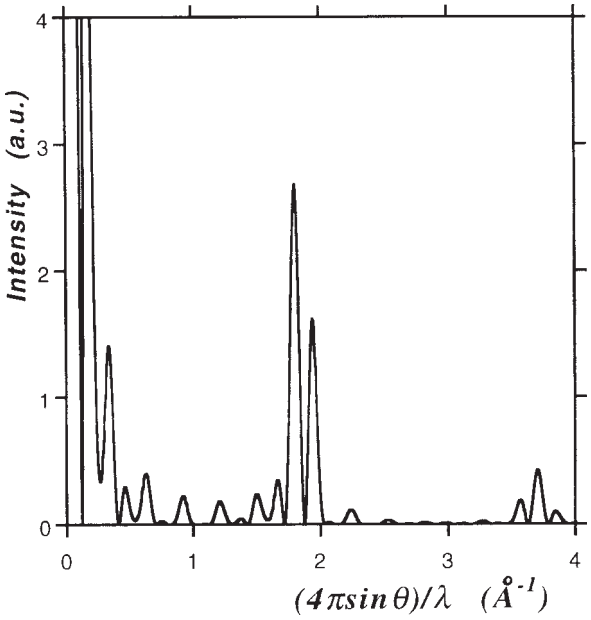

Figure 16. Simulated intensity distribution along the zeroth layer-line produced by the 7-layers nanotube of Figure 1c should be helpful in guiding and narrowing down the exploration of the "chirality space" of a nanotube.

---

of a set of initial atoms in the tubules. The (L_m,M_m) pairs should satisfy, up to a small tolerance of at most a few per cent, the condition that the circumference C_m given by equation (13) increases by $2\pi c_o$ / Å 8.81 from one tubule to the next in the set. Starting from an inner tubule of radius C_1, a possible tubule set can be read off the honeycomb lattice of Figure 15 in which successive concentric equidistant circles of radii C_m have been drawn. Any pair (L,M) representative of a lattice point sitting on or near (to within the tolerance) one of the circles, defines an acceptable tubule of the set. Figure 15 makes it clear that for fixed external dimensions C_1 and C_N of the nanotube, there can be several sets of tubules differing by their chirality (and handedness) and that the bigger the nanotube size, the larger this chirality degeneracy. The highly efficient diffraction formula for a complete tubule developed in this paper allows the simulation of the diffraction patterns corresponding to all possible chirality sequences compatible with the above construction rules. The observed TEM/ED chirality map discussed before (Bernaerts *et al.*, 1996).

When two or more coaxial tubules are considered, interferences are expected from adding the complex diffraction amplitudes of individual tubules. Three sets of parameters are expected to govern interference effects: (i) the new characteristic distance c_o Å 0.34 nm will produce periodic reinforcements of diffracted intensities in the direction normal to the nanotube axis; (ii) different chirality sequences will lead not only to different spot patterns but also to different, nonadditive spot intensities; (iii) changing the relative tubule registry by gliding or rotating the tubules with respect to each other about their common axis should also affect the spot intensities. In this paper, we will explore only the first two effects.

We can easily predict the major interference effect associated with the interlayer distance c_o. Indeed we expect a constructive interference when $k_\perp$ Å $2\pi n/c_o$ along the zeroth order layer-line where n is a nonzero integer. If all the tubule radii r_m are much larger than c_o, the arguments of the Bessel functions in equation (10) will be large as soon as we leave the center of the diffraction pattern towards the first order circle: $k_\perp r_m$ Å $2\pi n r_m / c_o = C_m n / c_o$ Å 13n for, say, an (18,0) tubule. We can then make use of the approximate expression of the dominant Bessel function $J_o(x)$ for large argument $x = k_\perp r$ (Abramowitch and Stegun, 1984): $J_o(x)$ Å $\cos(x-\pi/4)$. Adding the various terms for tubule radii $r_m = r_1 + m\, c_o$, we see that the phase in the cosine changes by 2π from one tubule to the next. Ignoring the slow decrease of the J_o oscillation ampli-tudes, the end result is a total amplitude at $k_\perp = 2\pi n/c_o$ growing like the number N of tubules and the intensity of the (0002n) spot growing like N^2. This quantitatively explains the appearance of the (0002n) sets of spots as the principal feature in the diffraction pattern of every multilayer nanotube. Figure 16 confirms this behavior. It shows the intensity of the zeroth layer-line in the calculated diffraction pattern of Figure 1c. The nanotube comprises 7 tubules whose radii and chiralities (see the figure caption) have been chosen to simulate Figure 1a and the observed chiral angles of the diffraction pattern in Fig. 1b. The zeroth layer-line (Figs. 1c and 16) exhibits the predicted strong reinforcements corres-ponding to the observed (0002n) spots and, in addition, shows intervening

oscillations due to the interference of the two nanotube walls (the Young two-slits experiment). The agreement between simulated and observed patterns is not completely satisfactory but could certainly be improved by searching the chirality and registry space of the 7-layers nanotube, as explained before.

Discussion

This paper has presented a short review of TEM-ED observations of straight and coiled nanotubes. In the description of the observed patterns, the emphasis was put on the important characteristics which call for a quantitative theory of electron diffraction by nanotubes. Such a complete theory was developed for the straight nanotubes comprising any number of tubules of arbitrary chiralities and the simulated patterns based on this theory were successfully compared with the observed ones.

We wish to close this paper by pointing out a number of opportunities offered by the new theoretical approach.

The computer-efficient theory allows for the simulation of the diffraction by nanotubes with defects. For example atomic vacancies or vacancy clusters can be easily simulated by subtracting the amplitudes of the missing atoms from the perfect nanotube amplitude. Another example is the case of an "excentric" nanotube, i.e., having one or several missing layers which eventually produce anomalous lattice fringe spacings in the TEM image of the nanotube (Bernaerts *et al.*, 1996). This situation simply requires adding the amplitudes of non coaxial but parallel tubules.

Very recently, Thess *et al.* (1996) have succeeded in producing, by carbon laser ablation, "ropes" of monodispersed, parallel (10,10) perpendicular tubules and have taken a powder XRD diagram of the material. The present theory is ideally suited to compute the fiber and powder diagram of such a system since it provides the exact tubule molecular form factor from which to calculate the diffraction of the ordered triangular lattice of tubules in the "rope".

Other helical structures of light elements such as the carbon conical scrolls (Amelinckx *et al.*, 1992) and the BN and BCN nanotubes recently discovered (Tenne, 1995; Stephan *et al.*, 1994) are ameanable to an application of the present theory since they can be described as an ensemble of regular helices. The theory will also be found useful for interpreting X-ray diffraction data from nanotubes made of heavy elements such as the disulfide MoS_2, WS_2 (e.g., Tenne, 1995).

Certain fundamental extensions of the theory are required to deal with coiled nanotubes. Since these are made up from connected pieces of straight cylindrical segments, it will be necessary to account for the finite length of the straight sections and of the irregular atomic arrangement in the connecting knee regions which contain ring defects (Ivanov *et al.*, 1994). The latter must be introduced numerically, atom by atom, while the former can be handled analytically via equations (4) and (5) in which the δ-function is replaced by a slit-function giving the diffraction amplitude of a helix of finite length.

Nanotubes containing cylindrical scrolls (Amelinckx *et al.*, 1995b) pose a special simulation problem. They require the diffraction amplitude of helices of finite length wound around a circular cone. This can be written analytically and involves derivatives of the cylindrical Bessel functions (Abramowitz and Stegun, 1984). Work along these lines is in progress.

Acknowledgements

We thank Dr. S. Iijima for allowing the reproduction of Figures 1a,b and Dr. Qin for informing us about his work (Qin, 1994). We are grateful for the support of the following agencies: the Belgian National Science Foundation, the Ministry of Sciences, the European Commission HCM program, the Walloon Government.

References

Abramowitz M, Stegun IA (1984) Pocketbook of Mathematical Functions. Verlag Harri Deutsch, Frankfurt, p. 108.

Amelinckx S, Luyten W, Krekels T, Van Tendeloo G, Van Landuyt J (1992) Conical helically wound, graphite whiskers: a limiting member of the "fullerenes?". J. Cryst. Growth **121**, 543-558.

Amelinckx S, Zhang XB, Bernaerts D, Zhang XF, Ivanov V. B'Nagy J (1994) A formation mechanism for catalytically grown shaped graphite nanotubes. Science **265**, 635-639.

Amelinckx S, Bernaerts D, Van Tendeloo G, Van Landuyt J, Lucas AA, Mathot M, Lambin Ph (1995a) The morphology, structure and texture of carbon nanotubes: an electron microscopy study. In: Physics and Chemistry of Fullerenes and Derivatives. Kuzmany H, Fink J, Mehring M, Roth S (eds.). World Scientific, Singapore, pp. 515-541.

Amelinckx S, Bernaerts D, Zhang X.B, Van Tendeloo G, Van Landuyt J (1995b) A structure model and growth mechanism for multishell carbon nanotubes. Science **267**, 1334-1338.

Arfken G (1985) Mathematical Methods for Physicists, Academic Press, N.Y., p. 585.

Bacsa WS, De Heer WA (1995) Optical properties of aligned carbon nanotubes. In: Physics and Chemistry of Fullerenes and Derivatives. Kuzmany H, Fink J, Mehring M, Roth S (eds.). World Scientific, Singapore, pp. 574-577.

Baker RTK (1989) Catalytic growth of carbon filaments. Carbon **27**, 315-323.

Bernaerts D, Zhang XB, Zhang XF, Amelinckx S, Van

Tendeloo G, Van Landuyt J, Yvanov V, B'Nagy J (1995a) Electron microscopy study of coiled carbon nanotubules. Phil. Mag. **A71**, 605-630.

Bernaerts D, Amelinckx S, Op de Beeck M, Van Tendeloo G, Van Landuyt J (1996) The chirality of carbon nanotubules determined by dark field electron microscopy. Phil. Mag. **74**, 723-740.

Bernaerts D, Lucas A, Amelinckx S (1997) On a peculiar contrast effect associated with carbon nano-tubes, Phil. Mag. **76**, 267-270.

Bethune DS, Kiang CH, de Vries MS, Gorman G, Savoy R, Vazquez J, Beyers R (1993) Cobalt-catalysed growth of carbon nanotubes with single-atomic-layer walls. Nature **363**, 605-607.

Charlier J-C, Michenaud J-P (1993), Energetics of multilayered carbon tubules. Phys. Rev. Lett. **70**, 1858-1861.

Cochran W, Crick FHC, Vand V (1952) The structure of synthetic polypeptides. I. The transform of atoms on a helix. Acta Cryst. **5**, 581-586.

Colbert D, Smalley RE (1995) Electric effects in nanotube growth. Carbon **33**, 921-924.

Colbert DT, Zhang J, McClure SM, Nikolaev P, Chen Z, Hafner JH, Owens DW, Kotula PG, Carter CB, Weaver JH, Rinzler AG and Smalley RE (1994) Growth and sintering of fullerene nanotubes. Science **266**, 1218-1222.

de Heer WA, Bacsa WS, Châtelain A, Gerfin T, Humphrey-Baker R, Forro L, Ugarte D (1995) Aligned carbon nanotube films: Production, optical and electronic properties. Science **270**, 1179-1180.

Doyle PA, Turner PS (1968) Relativistic Hartree-Fock X-ray and electron scattering factors. Acta Cryst. **A24**, 390-397.

Dresselhaus MS, Dresselhaus G, Suguhara K, Spain IL, Goldberg HA (1988) Graphite Fibers and Filaments. Springer Series in Materials Science. Vol. 5, Springer-Verlag, Berlin.

Dresselhaus MS, Dresselhaus G, Saito R (1992) Carbon fibers based on C_{60} and their symmetry. Phys. Rev. **B45**, 6234-6242.

Dresselhaus MS, Dresselhaus G, Saito R (1995) Physics of carbon nanotubes. Carbon **33**, 883-891.

Dunlap BI (1992) Connecting carbon tubules. Phys. Rev. **46**, 1933-1936.

Dunlap BI (1994) Relating carbon tubules. Phys. Rev. **49**, 5643-5651.

Ebbesen TW (1994) Carbon nanotubes. Annu. Rev. Mater. Sci. **24**, 235-264.

Ebbesen TW, Ajayan PM (1992) Large-scale synthesis of carbon nanotubes. Nature **358**, 220-222.

Ebbesen TW, Ajayan PM, Hiura H, Tanigaki K (1994) Purification of nanotubes. Nature **367**, 519-519.

Finch JT (1972) The hand of the helix of Tobacco Mosaic Virus. J. Mol. Biol. **66**, 291-294.

Fonseca A, Hernadi K, B'Nagy J, Lambin Ph, Lucas AA (1995) Model structure of perfectly graphitizable coiled carbon nanotubes. Carbon **33**, 1759-1775.

Franklin RE, Gosling RG (1953) Molecular configuration in sodium thymonucleate. Nature **171**, 740-741.

Gamaly EG, Ebbesen Th (1995) On the mechanism of carbon nanotube formation in the arc-discharge. In: Physics and Chemistry of Fullerenes and Derivatives. Kuzmany H, Fink J, Mehring M, Roth S (eds.). World Scientific, Singapore, p. 546-550.

Gevers R (1970) Kinematical theory of electron diffraction. In: Modern Diffraction and Imaging Techniques in Material Science. Amelinckx S, Gevers R, Remaut G, Van Landuyt J (eds.). North Holland, Amsterdam. p. 1.

Guo T, Nikolaev P, Thess A, Colbert DT, Smalley RE (1995a) Catalytic growth of single-walled nanotubes by laser vaporization. Chem Phys Lett **243**, 49-54.

Guo T, Nikolaev P, Rinzler A, Tomanek D, Colbert D, Smalley RE (1995b) Self-assembly of tubular fullerenes. J. Phys. Chem. **99**, 10694-10697.

Hamada N, Sawada S, Oshiyama A (1992) New one-dimensional conductors: graphitic microtubules. Phys. Rev. Lett. **68**, 1579-1581.

Henrard L, Senet P, Lambin Ph, Lucas AA (1996) On the ultraviolet spectrum of multishell fullerenes and its role as possible component of interstellar dust. Full. Sci. Technol. **4**, 131-163.

Hiura H, Ebbesen TW, Tanigaki K, Takahashi H (1993) Raman studies of carbon nanotubes. Chem. Phys. Lett. **202**, 509-512.

Hsu WK, Hare JP, Terrones M, Kroto HW, Walton DRM, Harris PJF (1995) Condensed-phase nanotubes. Nature **377**, 687-689.

Ihara S, Itoh S, Kitakami JI (1993) Helically coiled cage forms of graphitic carbon. Phys. Rev. **48**, 5643-5647.

Iijima S (1991) Helical microtubules of graphitic carbon. Nature **354**, 56-58.

Iijima S, Ichihashi T (1993) Single-shell carbon nanotubes of 1-nm diameter. Nature **363**, 603-605.

Itoh S, Ihara S (1993) Toroidal forms of graphitic carbon. II. Elongated tori. Phys. Rev. **48**, 8323-8328.

Ivanov V, B'Nagy J, Lambin Ph, Lucas A, Zhang XB, Zhang XF, Bernaerts D, Van Tendeloo G, Amelinckx S, Van Landuyt J (1994) The study of carbon nanotubules produced by catalytic method. Chem. Phys. Lett. **223**, 329-335.

José-Yacaman M, Miki-Yoshida M, Rendon L, Stantiesteban JG (1993) Catalytic growth of carbon microtubules with fullerene structure. Appl. Phys. Lett. **62**, 202-204.

Kawaguchi M, Nozaki K, Motojima S, Iwagana H (1992) A growth mechanism of regularly coiled carbon fibers through acetylene pyrolysis. J. Cryst. Growth **118**, 309-312.

Klein DJ, Seitz WA, Schmaltz TG (1993) Symmetry of infinite polymers: application to buckytubes. J. Phys. Chem.

97, 1231-1236.

Klug A, Crick FHC, Wyckoff HW (1958) Diffraction by helical structures. Acta Cryst. **11**, 199-213.

Krätschmer W, Lamb LD, Fostiropoulos K, Huffman DR (1990) Solid C60: a new form of carbon. Nature **347**, 354-358.

Kroto HW, Heath JR, O'Brien SC, Curl RF, Smalley RE (1985) C60: Buckminsterfullerene. Nature **318**, 162-163.

Lambin Ph, Fonseca A, Vigneron JP, B'Nagy J, Lucas AA (1995) Structural and electronic properties of bent carbon nanotubes, Chem. Phys. Lett. **245**, 85-89.

Landau L, Lifchitz E (1967) Mécanique Quantique (Quantum Mechanics). Edition Mir, Moscow, USSR, p. 565.

Langer L, Bayot V, Issi J-P, Stockman L, Van Haesendonck C, Bryunseraede Y, Heremans JP, Olk CH (1995) Electrical Resistivity of Carbon Nanotubes. In: Physics and Chemistry of Fullerenes and Derivatives. Kuzmany H, Fink J, Mehring M, Roth S (eds.). World Scientific, Singapore, p. 565-569.

Liu M, Cowley JM (1994a) Structures of the helical carbon nanotubes. Carbon **32**, 393-403.

Liu M, Cowley JM (1994b) Structures of carbon nanotubes studied by HRTEM and nanodiffraction. Ultramicroscopy **53**, 333-342.

Lucas AA, Bruyninckx V, Lambin Ph (1996) Calculating the diffraction of electrons or X-rays by carbon nanotubes. Europhys. Lett. **35**, 355-360.

Lu JP (1995) Novel magnetic properties of carbon nanotubes. Phys. Rev. Lett. **74**, 1123-1126.

Mintmire JW, Dunlap BI, White CW (1992) Are fullerene tubules metallic? Phys. Rev. Lett. **68**, 631-634.

Polanyi M (1921) Das Röntgen-Faserdiagramm. (The X-ray fiber diagram). Z. Phys. **7**, 149-180.

Qin LC (1994) Electron diffraction from cylindrical nanotubes, J. Mater. Res. **9**, 2450-2456.

Rich A (1992), Molecular recognition between protein and nucleic acids. In: The Chemical Bond. Zewail A (ed.). Academic Press, Boston, pp. 31-86.

Robertson DH, Brenner DH, Mintmire DW (1992) Energetics of nanoscale graphitic tubules. Phys. Rev. **B45**, 12592-12595.

Rodriguez NM (1993) A review of catalytically grown carbon nanofibers. J. Mater. Res. **8**, 3233-3250.

Smith GH, Burge RE (1962) The analytical representation of atomic scattering amplitudes for electrons. Acta Cryst. **15**, 182-186.

Stephan O, Ajayan PM, Colliex C, Redlich Ph, Lambert JM, Bernier P, Lefin P (1994) Doping graphitic and carbon nanotube structures with boron and nitrogen. Science **266**, 1683-1685.

Tenne R (1995) Doped and heteroatom-containing fullerene-like structures and nanotubes. Adv. Mat. **7**, 965-972, 989-995.

Thess A, Lee R, Nikolaev P, Dai H, Petit P, Robert J, Xu Ch, Lee YH, Kim SG, Colbert D, Scuseria G, Tomanek D, Fischer J, Smalley R (1996). Crystalline ropes of metallic carbon nanotubes. Science **273**, 483-487.

Vainshtein BK (1966) Diffraction of X-Rays by Chain Molecules. Elsevier, Amsterdam. pp. 150-151.

Verwerft M, Luyten W, Amelinckx S. (1990), Two remarkable defect related electron diffraction effects. Microsc. Microan. Microstruct. **1**, 167-173.

Watson J, Crick FHC (1953) A structure of deoxy-ribose nucleic acid. Nature **171**, 737-738.

White CT, Robertson DH, Mintmire JW (1993) Helical and rotational symmetries of nanoscale graphitic tubules. Phys. Rev. **B47**, 5485-5488.

Zhang XB, Zhang XF, Bernaerts D, Van Tendeloo G, Amelinckx S, Van Landuyt J, Ivanov V, B'Nagy J, Lambin Ph, Lucas A (1994) The texture of catalytically grown coil-shape carbon nanotubules. Europhys. Lett. **27**, 141-146.

Zhang XF, Zhang Z (1995) Polygonal spiral of coil-shaped carbon nanotubules. Phys. Rev. **B52**, 5313-5317.

Zhang XF, Zhang XB, Van Tendeloo G, Amelinckx S, Op de Beeck M, Van Landuyt J (1993a) Carbon nanotubes; their formation process and observation by electron microscopy, J. Cryst. Growth **130**, 368-382.

Zhang XF, Zhang XB, Amelinckx S, Van Tendeloo G, Van Landuyt J (1993b) The reciprocal space of carbon-tubes : a detailed interpretation of the electron diffraction effects, Ultramicroscopy **54**, 237-249.

Zhou O, Fleming RM, Murphy DW, Chen CH, Haddon RC, Ramirez AP, Glarum SH (1994) Deffects in carbon nano-structures. Science **263**, 1744-1747.

Discussion with Reviewers

M.S. Dresselhaus: In reading the paper I wanted to know how electron microscopy could distinguish between cylinders and scrolls.

Authors: The only, admittedly indirect, TEM evidence for scrolls is the observation (Bernaerts *et al*., 1995b) of anomalous spacings between basal lattice fringes in one wall or the other in the bright field image of a nanotube. The interpretation in terms of scrolls is consistent with the frequent finding that the number of distinct chiral angles is less than the number of tubules in a nanotube, a multiturn scroll having of course a constant chiral angle. One or several missing tubules in a nanotube would also lead to singular fringe spacings (Bernaerts *et al*., 1997) as a result of the van der Waals attraction of the inner portion of the nanotube towards the outer layers, although this interpretation would not explain the paucity of chiralities. The issue could be resolved by the chance imaging of a nanotube fragment along its axis.

M.S. Dresselhaus: I wonder whether resonances due to periodic stacking of nanotube arrays could be found. In view

of the interest in the single wall nanotubes produced by the Rice group (Thess *et al.*, 1996), some comments on what TEM can tell us about these materials would be of interest.
Authors: As stated the scattering amplitude of a single tubule will serve as the molecular form factor for the scattering by a tubule array, the total scattering amplitude being the product of the form factor by the Fourier transform of the two-dimensional array. A simplified form factor was used by Thess *et al.* (1996) to interpret their X-ray diffraction data from the triangular array of (10,10) tubules observed by the Rice group. Extinction of array resonances by the form factor are indeed observed (Thess *et al.*, 1996). Similar effects are expected for electron diffraction but have not been reported so far.

D.T. Colbert: Regarding the assignments made to the nanotube of Figure 1a from the simulation of Figure 1c, it is striking that the best simulation is for the first three layers to be of zig-zag type. Assuming that the (m,n) assignments are accurate, which I do not contest, do the authors have any explanation for this that would shed light on the growth mechanism? My own view is that the stabilizing adatom interactions between open edges first discussed in Guo *et al.* (1995a) is most effective for zero- and low-helicity zig-zag tubes (armchair layers are stabilized by the formation of C-C triple bonds along the "arms"). As layer diameters increase, this give way to the importance of finding the helicity that produces a diameter giving the best van der Waals interaction with neighboring layers, since the latter interaction grows as the square of the diameter. In addition, since adatom interlayer interactions were proposed to maintian the growing tip in an open state, keeping the *innermost* layers open is especially important; again, this is most effective for zig-zag layers.
Authors: We agree that atomic processes such as invoked by Guo *et al.* (1995a) and Thess *et al.* (1996) are likely to influence the choice of chirality sequence made by nature during growth. However, while the set of tubule diameters and chiral angles can be read off the experimental micrographs of Figures 1a and 1b, these micrographs give no direct information on the order in which the chiralities occur in the nanotube nor on the relative glide positions of the successive tubules. For the simulation of Figure 1c, the chirality sequence mentioned in the caption and zero glides were chosen rather arbitrarily as a first trial set and without attempting any optimization with the observed diffraction intensities.

J.M. Cowley: Have the authors found any evidence for the multi-walled carbon nanotubes of non-circular cross section found, for example, by Liu and Cowley (1994a)?
Authors: We have not found direct evidence of the polygonal cross section of tubules, even though we are convinced that polygonization must occur. By "polygonisation", we refer to the model proposed in Zhang *et al.* (1993a). The difference between circular and polygonized (18-20 sided polygon) in our sense is small and difficult to prove directly. This is different from the pentagonal model introduced by Liu and Cowley (1994a) to explain the singular c-fringe spacings. We attribute these anomalous spacings (Amelinckx *et al.*, 1995b) to the presence of dislocation-like defects (scrolls with ending of graphene sheets).

J.M. Cowley: The dark-field method used by Bernaerts *et al.* (1996) should be a very effective one. Do their results confirm the conclusion of Liu and Cowley (1994b), that in a multi-walled nanotube the chirality changes after every three or four graphitic sheets?
Authors: Our scroll model for the anomalous fringe spacings provides at the same time an explanation for the problem raised by this question. We do confirm that the number of different chiral angles within a multishell tube is three to four times smaller than the number of shells.

J.M. Cowley: The arguments made regarding the validity of the kinematical approximation for transmission through graphitic sheets or for diffraction from ordered graphite crystals under two-beam diffraction conditions do not seem to be directly relevant to the case of nanotubes for which the important consideration is the scattering by the graphitic layers in the tube walls which are nearly parallel to the incident beam. Have the authors considered the projected potential distributions from the weak-phase-object approximation which leads to asymmetries in the diffraction pattern, as observed by Cowley *et al.* (1996)?
Authors: We agree that considerations on planar graphitic sheets or crystalline graphite are not quantitatively applicable to the curvilinear geometry of nanotubes. However, a full dynamical theory of diffraction by the latter is not yet available and the former systems were therefore considered for an order-of-magnitude evaluation of the scattering power of nanotubes. We believe that this evaluation was necessary to test the applicability of the first Born approximation. Regarding the asymmetries in the (00l) diffraction intensities it appears that such asymmetries could be discovered by Cowley *et al.* (1996) with the use of "nano-beams", i.e., electron beams of diameter of the order of one nm or less. We have not considered this situation since the electron beams used in the work described in the present paper covers several hundred Å. The a-symmetries we observed in this case (Bernaerts *et al.*, 1997) occur between the (00l)-constructed dark-field images of the left and the right walls of a circular nanotube. These asymmetries, which we attribute again to the presence of singular fringe spacings in one nanotube wall, are unrelated to those observed by Cowley *et al.* (1996).

Additional References

Bernaerts D, Amelinckx S, Zhang XB, Van Tendeloo G, Van Landuyt J (1995) Structural aspects of carbon nanotubes. In: Physics and Chemistry of Fullerenes and Derivatives. Kuzmany H, Fink J, Mehring M, Roth S (eds.). World Scientific, Singapore, pp. 551-555.

Cowley JM, Packard SD, Scott D (1996) Coherent nano-diffraction from phase objects: carbon nanotubes. Ultramicroscopy **63**, 39-47.